Magn Reson Med Sci 2022; 21; 212–234
doi:10.2463/mrms.rev.2020-0184 Published Online: April 29, 2021

REVIEW

An Invited Review for the Special 20th Anniversary Issue of MRMS

State-of-the-art MR Imaging for Thoracic Diseases

Yumi Tanaka[1], Yoshiharu Ohno[*1,2], Satomu Hanamatsu[1], Yuki Obama[1], Takahiro Ueda[1], Hirotaka Ikeda[1], Akiyoshi Iwase[3], Takashi Fukuba[3], Hidekazu Hattori[1], Kazuhiro Murayama[2], Takeshi Yoshikawa[4], Daisuke Takenaka[4], Hisanobu Koyama[5], and Hiroshi Toyama[1]

Since thoracic MR imaging was first used in a clinical setting, it has been suggested that MR imaging has limited clinical utility for thoracic diseases, especially lung diseases, in comparison with x-ray CT and positron emission tomography (PET)/CT. However, in many countries and states and for specific indications, MR imaging has recently become practicable. In addition, recently developed pulmonary MR imaging with ultra-short TE (UTE) and zero TE (ZTE) has enhanced the utility of MR imaging for thoracic diseases in routine clinical practice. Furthermore, MR imaging has been introduced as being capable of assessing pulmonary function. It should be borne in mind, however, that these applications have so far been academically and clinically used only for healthy volunteers, but not for patients with various pulmonary diseases in Japan or other countries. In 2020, the Fleischner Society published a new report, which provides consensus expert opinions regarding appropriate clinical indications of pulmonary MR imaging for not only oncologic but also pulmonary diseases. This review article presents a brief history of MR imaging for thoracic diseases regarding its technical aspects and major clinical indications in Japan 1) in terms of what is currently available, 2) promising but requiring further validation or evaluation, and 3) developments warranting research investigations in preclinical or patient studies. State-of-the-art MR imaging can non-invasively visualize lung structural and functional abnormalities without ionizing radiation and thus provide an alternative to CT. MR imaging is considered as a tool for providing unique information. Moreover, prospective, randomized, and multi-center trials should be conducted to directly compare MR imaging with conventional methods to determine whether the former has equal or superior clinical relevance. The results of these trials together with continued improvements are expected to update or modify recommendations for the use of MRI in near future.

Keywords: *thorax, lung, mediastinum, magnetic resonance imaging*

Introduction

Since thoracic MR imaging was first used in a clinical setting, it has been suggested that MR imaging has limited clinical utility for thoracic diseases, especially lung diseases, in comparison with x-ray CT and positron emission tomography (PET)/CT. This is because in 1991, the Radiologic Diagnostic Oncology Group (RDOG) report concluded the advantage of MR imaging for lung cancer staging was limited compared with that of CT.[1] However, in a number of countries and states and for specific indications, MR imaging has recently become practicable due to advances in MR pulse sequences, multi-coil parallel imaging and acceleration methods, utilization of contrast media, and application of promising post-processing software or analysis methods. In

[1]Department of Radiology, Fujita Health University School of Medicine, Toyoake, Aichi, Japan
[2]Joint Research Laboratory of Advanced Medical Imaging, Fujita Health University School of Medicine, Toyoake, Aichi, Japan
[3]Department of Radiology, Fujita Health University Hospital, Toyoake, Aichi, Japan
[4]Department of Diagnostic Radiology, Hyogo Cancer Center, Akashi, Hyogo, Japan
[5]Department of Radiology, Osaka Police Hospital, Osaka, Osaka, Japan
[*]Corresponding author: Department of Radiology, Fujita Health University School of Medicine, 1-98, Dengakugakubo, Kutsukakecho, Toyoake, Aichi 470-1192, Japan. Phone: +81-562-93-9259, Fax: +81-562-95-2253, E-mail: yohno@fujita-hu.ac.jp

Received: December 25, 2020 | Accepted: March 4, 2021

Table 1 Summary of recommended clinical indications of MR imaging for thoracic diseases

Category	Clinical Indications
Suggested for currently available application	lung cancer staging (TNM stating)
	pulmonary nodule characterization
	pulmonary nodule detection
	pulmonary hypertension
	pulmonary thromboembolism
Promising but requiring further validation or evaluation (see Supplement Materials)	radiological finding evaluation in pulmonary parenchymal diseases
Warranting research investigations (see Supplement Materials)	chronic obstructive pulmonary disease (COPD)
	asthma
	interstitial lung disease

COPD, chronic obstructive pulmonary disease.

addition, recently developed pulmonary MR imaging with ultra-short TE (UTE) and zero TE (ZTE) has enhanced the utility of MR imaging for thoracic diseases in routine clinical practice. It has also been suggested that MR imaging is capable of assessing pulmonary function. Furthermore, MR imaging with inhaled gas methods, such as hyperpolarized noble gas and fluorine gas, has been introduced as another MR method for assessing pulmonary function. It should be borne in mind, however, that these applications have so far been academically and clinically used only for healthy volunteers, but not for patients with various pulmonary diseases in Japan or other countries.

In 2020, the Fleischner Society published a new report, which provides consensus expert opinions regarding appropriate clinical indications of pulmonary MR imaging for not only oncologic but also pulmonary diseases.[2] In addition, 2021 is the 20th anniversary of the founding of Magnetic Resonance in Medical Science, which is the official journal of the Japanese Society of Magnetic Resonance in Medical Science, publishing scientific reports with advanced MR information from researchers in Japan, as well as in other countries. Currently, MR imaging for thoracic diseases is considered to be one of the most attractive research fields and represents a new frontier in MR imaging. Consequently, presentations at numerous annual meetings of various societies, such as the International Society of Magnetic Resonance in Medicine, the Radiological Society of North America, and the European Society of Radiology, have increased because many investigators are conducting tests in both academic and clinical settings in many parts of the world. In this review article, we, therefore, present a brief history of MR imaging for thoracic diseases regarding its technical aspects and major clinical indications in Japan 1) in terms of what is currently available, 2) promising but requiring further validation or evaluation, and 3) developments warranting research investigations in preclinical or patient studies. Clinical indications recommended in this article for current application are based on strong evidence provided in four or more publications from multiple institutions conducting clinical studies of more than 100 patients. In addition, these targets are considered as appropriate indications in many Western countries including USA and refunded by health insurances in all over the world. On the other hand, clinical indications referred to as promising but requiring further validation or evaluation refer to those introduced in two to three publications and using less than 100 patients and data sets. Finally, clinical indications referred to as appropriate for research investigations in clinical or patient studies do not meet the above criteria or are limited to preclinical research. Table 1 summarizes these clinical indications based on our experience and those published in the Fleischner Society Position paper.[2,3] In addition, clinical indications suggested as 2) promising but requiring further validation or evaluation and 3) developments warranting research investigations in preclinical or patient studies are stated as Supplement materials.

Brief History of Thoracic MR Imaging Techniques

Paul Lauterbur developed the first MRI scanner in 1970s, for which he and Peter Mansfield received the 2003 Nobel Prize in Physiology or Medicine. Thoracic MR imaging for the assessment of lung parenchyma diseases, as well as thoracic oncologic diseases, was first tested in the 1990s.[2–32] As early as 1991, however, RDOG reports concluded that MR imaging had less utility for TNM staging in lung cancer than CT. In addition, several investigators reported that MR imaging was less capable of providing evidence of lung parenchyma than CT.[4–8]

Inhomogeneity of magnetic susceptibility resulting from air and soft tissue interfaces within the lung, combined with

motion and low intrinsic proton density, has hindered the use of MR imaging for lung parenchyma. The large difference in magnetic susceptibility between air and lung parenchyma results in broad frequency distributions and phase dispersion within voxels, thus causing an incoherent proton spectrum and noise after image reconstruction as well as short T2 star (T2*).[33–35] Moreover, the discrepancy in susceptibility to artifacts between lung parenchyma and the chest wall manifests as a dark line perpendicular to the frequency encoding direction. In view of these issues, many investigators have been trying to establish the utility of MR imaging for thoracic diseases during the last few decades.

Clinical MR imaging for thoracic diseases was performed by means of spin-echo (SE) sequence in the early 1990s, and attempts were made to use turbo or fast SE and gradient-recalled-echo (GRE) sequences in the mid-1990s. Furthermore, fast GRE with short echo time (TE), in- and opposed phase T1-weighted GRE, T1- and T2-weighted, and short inversion time (TI) inversion recovery (STIR) turbo SE with half-Fourier single-shot method with and without black-blood technique had been used in routine clinical practice since the early 1990s.[2–32,36–40] In addition, diffusion-weighted imaging (DWI) has been utilized in combination with single-shot echo-planar imaging (EPI) sequence and the fat suppression technique for oncologic patients since 2004.[18,20,21,24,30,41,42] Therefore, almost all sequences for MR imaging for thoracic oncologic diseases were established between the early 1990s and 2004.

During the same period, the parallel imaging technique, as well as fast GRE with short TE or ultra-short TE using contrast media, was proposed for time-resolved (or 4D) contrast-enhanced (CE) MR angiography or dynamic CE-perfusion MRI, while investigations were started of velocity-encoded (or phase-encoded) MR imaging for pulmonary vascular diseases, as well as thoracic oncology in routine clinical practice.[2,3,18,25,27,28,31]

The recently introduced radial acquisition of k-space data from free induction decay (FID) can reduce TE to less than 200 μs, thus minimizing signal decay caused by short transverse relaxation time (T2/T2*). It has, therefore, been suggested that the development of UTE or ZTE sequences could be a game changer for pulmonary MR imaging[32,43–48] because the UTE sequence allows for better visualization of the endogenous MR signal of lung parenchyma than can be obtained with the conventional short echo image sequence.[2,3,32,43] It has also been suggested that MR imaging with UTE can make it possible to quantitatively assess the regional T2* values and morphological changes in pulmonary parenchymal diseases.[32,43–53]

Furthermore, hyperpolarized noble gas MR imaging with helium-3 (^{3}He) and xenon-129 (^{129}Xe), oxygen- (O_2-) enhanced MR imaging, and fluorine-19 (^{19}F-) MR imaging has been recommended since the 1990s for use in pulmonary functional MR imaging techniques, such as non-CE- and dynamic CE-perfusion MR imaging.[10,12,13,15,17,22,23,25,27,28,31] O_2-enhanced MR imaging and non-CE- and dynamic CE-perfusion MR imaging are now in clinical global use for various pulmonary diseases, although hyperpolarized noble gas MR imaging and ^{19}F-MR imaging are still being tested at a limited number of institutions in a few countries.[9,12,13,15,17,22,23,25,27,28,30] However, other gases besides oxygen are not currently available for routine clinical practice because of the following reasons: they have not received the U.S. Food and Drug Administration (FDA) approval, the limited clinical availability of such gases due to their total amounts being limited, and their high cost. In addition, all gas MR techniques, except for O_2-enhanced MR imaging, require special equipment such as polarizer, transmitter, and receiver coils with multiple nuclear resonance capability.[9,12,13,15,17,22,23,25,27,28,30] Therefore, proton-based MR imaging, including non-CE- and CE-MR angiography as well as perfusion MR imaging and O_2-enhanced MR imaging, is the only method that can be currently used in routine clinical practice anywhere in the world.

In conjunction with dedicated thoracic MR imaging, the addition, since the middle of this century's first decade, of multiple surface coils with parallel imaging capability and a moving table has made it possible to obtain whole-body MR imaging with and without DWI for not only pulmonary vascular diseases with deep venous thrombosis (DVT) but also various oncologic diseases, including lung cancer, thymic epithelial tumor, malignant lymphoma, and mesotheliomas.[18,20,21,24,28,30] In addition, recently developed positron emission tomography using fluorine-18-fluorodeoxyglucose (FDG) fused with MR imaging (FDG-PET/MRI or FDG-MR/PET) has been tested to ascertain its clinical utility for TNM staging and recurrence evaluation in the above-mentioned diseases, and attempts have been made to evaluate not only MR-based but also glucose metabolism-based information with the same examination.[16,18,20,21,24,30,54–64] These new techniques may, therefore, be put to better use for one-stop shopping examinations and should be considered promising tools for the assessment of thoracic oncologic patients.

The above-mentioned advancements have resulted in a wider clinical utilization of MR imaging for thoracic diseases while its use for many thoracic diseases are covered by health insurance in Europe, Korea, and USA, although it is still limited in Japan. The principal reasons for this delay in Japan are the speed, availability, familiarity, ease of access, superb natural contrast, and high resolution of the lung parenchyma provided by thin-section CT. Other reasons for the delayed clinical use of MR imaging for thoracic diseases include its longer acquisition time, respiratory motion, and the lung's lower proton density and the aforementioned effects on magnetic susceptibility resulting from air–soft tissue interfaces. Nevertheless, MR imaging appears to be poised to become the primary clinical imaging modality for specific indications as detailed below.

Fig. 1 64-year-old male with a solid nodule with 13-mm-long axis diameter and diagnosed as invasive adenocarcinoma (From left to right: standard-dose CT, low-dose CT, and pulmonary MR imaging with UTE). Standard- and low-dose CTs and pulmonary MR imaging with UTE clearly show a solid nodule with a 13-mm-long axis diameter in the right upper lobe. (Reproduced, with permission, from reference No. 45) UTE, ultra-short TE.

Fig. 2 60-year-old male with part-solid nodule with 15-mm-long axis diameter and diagnosed as invasive adenocarcinoma (From left to right: standard-dose CT, low-dose CT, and pulmonary MR imaging with UTE). Standard- and low-dose CTs and pulmonary MR imaging with UTE clearly show a part-solid nodule with a 15-mm-long axis diameter in the right upper lobe. (Reproduced, with permission, from reference No. 45) UTE, ultra-short TE.

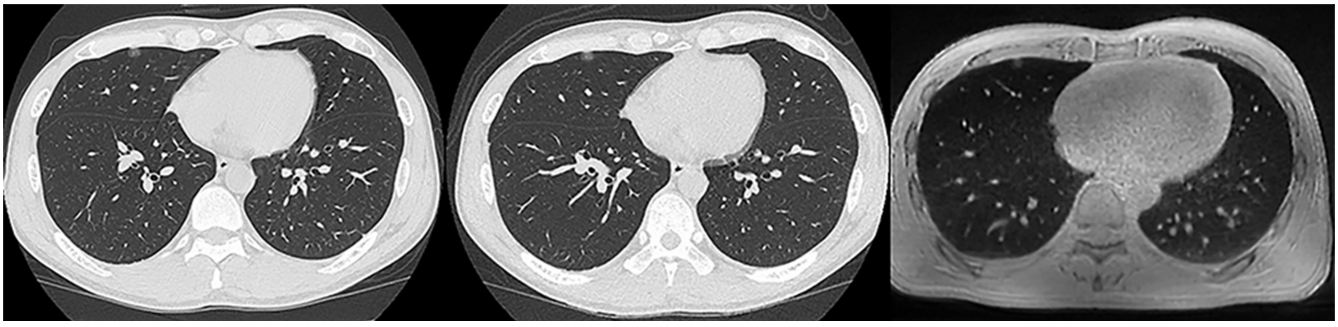

Fig. 3 48-year-old male with ground-glass nodule, 5-mm-long axis diameter, and followed up for over 1 year (From left to right: standard-dose CT, low-dose CT, and pulmonary MR imaging with UTE). Standard- and low-dose CTs and pulmonary MR imaging with UTE clearly show a ground-glass nodule with a 5-mm-long diameter in the right middle lobe. (Reproduced, with permission, from reference No. 45) UTE, ultra-short TE.

Clinical Indications Suggested for Currently Available Techniques

Pulmonary nodule detection and characterization

Lung cancer detection and pulmonary nodule characterization are major challenges for chest radiologists. While chest radiography or CT is utilized for lung cancer or nodule detection, MR imaging can contribute to specific clinical scenarios. Detection rates of some MR techniques, such as SE and turbo SE sequences including STIR and GRE sequences, studied and applied during the last few decades, reportedly ranged from 26% to 96%.[44–46,65–71] Since 2016, for 3D GRE sequencing with UTE of less than 200 μs, a detection rate of > 90% has been reported for non-solid, part-solid, and solid nodules ranging from 4 to 29 mm in diameter, thus challenging standard- and reduced-dose thin-section CT for nodule detection (Figs. 1–3).[45] In addition, evaluation of radiological findings also suggests that there is no significant difference in capability between

thin-section CT and thin-section pulmonary MR imaging with UTE.[44–46] Finally, nodule detection with MR imaging as a screening tool was recently compared with that of low-dose CT.[45,48] Therefore, pulmonary MR imaging with UTE is considered as a promising sequencing technique in this setting and can play a complementary role in the management of pulmonary nodules in routine clinical practice. Table 2 shows major results for previously reported nodule detection capability by MR imaging.

When a nodule or mass is detected on a chest radiograph, CT, or MR imaging, clinical interest is shifted to further examination for pulmonary nodule characterization, and numerous MR sequences have been evaluated for this purpose.[19] Currently, DWI is considered the most useful, with a meta-analysis pooled sensitivity and specificity of 83% and 80%, respectively.[72] When DWI and FDG-PET/CT were compared in a meta-analysis for diagnosis of the same nodule, DWI yielded an AUC of 0.93 versus 0.86 for FDG-PET/CT ($P < 0.001$). This meta-analysis also showed that the diagnostic odds ratio for DWI was significantly superior to that for FDG-PET/CT ($P = 0.001$).[73] Furthermore, it has been suggested that DWI has the potential to differentiate between malignant and benign nodules by means of different DWI indexes, such as apparent diffusion coefficient (ADC), lesion-to-spinal cord ratio (LSR) at different b value or e intravoxel incoherent motion (IVIM)-based information.[74–76] Therefore, currently available data show that DWI can be considered at least as valuable as FDG-PET/CT for pulmonary nodule or mass characterizations in routine clinical practice.

As a result of advances in MR systems and pulse sequences, there are now three major methods available for dynamic MR imaging of the lung. Many investigators have proposed that dynamic MR imaging be used for 2D SE or turbo SE sequences or for various types of 2D or 3D GRE sequences and that enhancement patterns within nodules and/or parameters determined from signal intensity–time course curves be assessed visually. These curves represent the first transit and/or recirculation and washout of contrast media under breath holding or repeated breath holding during a period of less than 10 min.[11,14,16,18–21,25,29,30,77–86] In addition, there are various dynamic MR techniques for distinguishing malignant from benign nodules with reported sensitivities ranging from 52% to 100%, specificities from 17% to 100%, and accuracies from 58% to 96%,[11,14,16,18–21,25,29,30,77–86] while a meta-analysis reported that there were no significant differences in diagnostic performance among dynamic CE-CT, dynamic CE-MR imaging, FDG-PET, and single photon emission computed tomography (SPECT).[87] However, dynamic MR imaging with the 3D GRE sequence and ultra-short TE, which requires less than 30-sec breath holding for acquisition of all data, has demonstrated its superior diagnostic performance in a direct and prospective comparison study of dynamic CE-CT and FDG-PET/CT or other modalities (Fig. 4).[82,85,86] It was also found that completion of FDG-PET or PET/CT takes almost 2 hours after injection of FDG. Dynamic MR imaging may thus be able to play a complementary or substitutional role in the characterization of solitary pulmonary nodules (SPNs) assessed with dynamic CE-CT, FDG-PET, and/or PET/CT. Table 3 shows major study results for diagnosis of pulmonary nodules by means of dynamic CE-MR imaging.

Lung cancer staging (TNM Staging)

When a nodule or mass is diagnosed as malignant, clinicians focus on TNM (i.e. Tumor, Node, and Metastasis) staging by using CT and FDG-PET/CT, while MR imaging is also used for answering some clinical questions not only in Europe, China, Japan, Korea, and Taiwan but also in the United States, where it was recently decided that the cost of MR imaging can be covered by health insurance. MR imaging was originally proposed for T factor evaluations,[1,88–90] and STIR turbo SE imaging and DWI were subsequently proposed to perform a complementary function for N factor assessment of non-small cell lung cancer (NSCLC) more effectively in comparison with CT and FDG-PET/CT.[91–103] In addition, STIR turbo SE imaging was also introduced as more sensitive and accurate than DWI and FDG-PET/CT (Figs. 5 and 6).[99,100] When both MR imaging and FDG-PET/CT data are available, the inclusive criteria of MRI or FDG-PET/CT help significantly improve the sensitivity for detecting nodal metastasis compared with that of FDG-PET/CT alone and may reduce unnecessary open thoracotomy.[99] Furthermore, a meta-analysis disclosed better diagnostic performance for MR imaging than for FDG-PET/CT on a per-node and per-patient basis.[103] These findings, therefore, support the clinical relevance of MR imaging for N factor evaluation of NSCLC patients. Tables 4 and 5 show reported results for diagnostic performances of dedicated MR imaging for T and N factor assessments of NSCLC patients. These results indicate that the purpose of MR imaging may be shifting from T factor evaluation only to include N factor assessment in routine clinical practice.

Whole-body MR imaging, which can be performed with multiple array coils with parallel imaging capability and a moving table system, also provides accuracy and efficacy for NSCLC staging and recurrence evaluation comparable with that of FDG-PET/CT.[54–64,104–106] In addition, it has been suggested whole-body DWI can be useful for improving M stage evaluation capability for NSCLC patients.[56,57] It has also been reported that, while whole-body MR imaging is more useful for detecting brain and hepatic metastasis, FDG-PET/CT is more useful for detecting lymph node and soft-tissue metastasis.[54,55,58,104] In addition, whole-body MR imaging combined with PET (PET/MRI) has been found to be more useful for TNM staging of NSCLC and postoperative lung cancer recurrence than PET/CT or conventional radiological examinations (Table 6). This combination can thus be considered at least as effective as whole-body MR imaging when clinicians need to evaluate not only glucose metabolism-based information but also relaxation time-based information

Table 2 Capability of MR sequence for pulmonary nodule and mass detection determined in previous studies

	Year	Field strength (T)	Gold standard	Nodule size (mm)	Applied sequences	SE (%)	
Vogt FM, et al.[65]	2004	1.5	4-detector row CT	5 ≤	ECG-triggered, breath-hold proton density-weighted black blood-prepared HASTE	95.6	
Bruegel M, et al.[66]	2007	1.5	64-detector row CT	1–31	Breath-hold T2W HASTE	47.7	
					Breath-hold T2W IR-HASTE	45.5	
					Breath-hold T2W TSE	69.0	
					Breath-hold STIR	63.4	
					Precontrast 3D VIBE	54.1	
					Postcontrast 3D VIBE	51	
Yi CA, et al.[67]	2007	3	4-detector row CT	13–80	Respiratory- and pulse-triggered STIR	72.0	
					ECG-gated T1W 3D TSE	57.0	
					ECG-gated T2W triple inversion black blood TSE	56.0	
Koyama H, et al.[68]	2008	1.5	4-detector row CT	1–30	ECG-gated and respiratory-triggered T1W TSE	96.1	
					ECG-gated and respiratory-triggered T2W TSE	96.1	
					ECG-gated and respiratory-triggered STIR	96.1	
Frericks BB, et al.[69]	2008	1.5	16-detector row CT	1–61	Multi-breath-hold STIR	92.5	
					Respiratory-triggered T2W TSE	90.8	
					Postcontrast 3D VIBE	87.3	
Cieszanowski A, et al.[70]	2016	1.5	64-detector row CT	2–28	Breath-hold T1W VIBE	69.0	
					Breath-hold T1W opposed-phase GRE	48.7	
					Breath-hold T2W TSE	48.7	
					Breath-hold T2W TSE with SPAIR	54.9	
					Breath-hold T2W STIR	45.1	
					Breath-hold T2W HASTE	25.7	
Burris NS, et al.[71]	2016	3 (PET/MRI)	PET/CT with 16- or 64-detector row CTs	3–17	3D GRE with UTE	73.2	
					3D dual-echo GRE with a two-point Dixon method	30.5	
Ohno Y, et al.[45]	2017	3	64-detector row CT	4-29	Respiratory-gated 3D GRE with UTE	93.0	No significant difference with standard- and reduced dose CTs

ECG, electrocardiogram; GRE, gradient-echo; HASTE, half-fourier-acquisition single-shot turbo spin-echo; IR, inversion recovery; SE, sensitivity; SPAIR, spectral attenuated inversion recovery; STIR, short inversion time (TI) inversion recovery; T1W, T1-weighted; T2W, T2-weighted; TSE, turbo spin-echo; UTE, ultra-short TE; VIBE, volumetric interpolated breath-hold.

provided by PET/MRI.[60,61,64,65,105,106] However, when clinicians need to evaluate only glucose metabolism information based on FDG uptake, findings indicate that the diagnostic performance of PET/MRI as almost equal to that of PET/CT for TNM staging and recurrence evaluation of lung cancer patients in routine clinical practice.[60,61,64,65,105,106] Therefore, whole-body MR imaging, as well as FDG-PET/MRI, may function as a substitute for FDG-PET/CT and deserves to be more frequently used for the management of lung cancer patients in routine clinical practice.

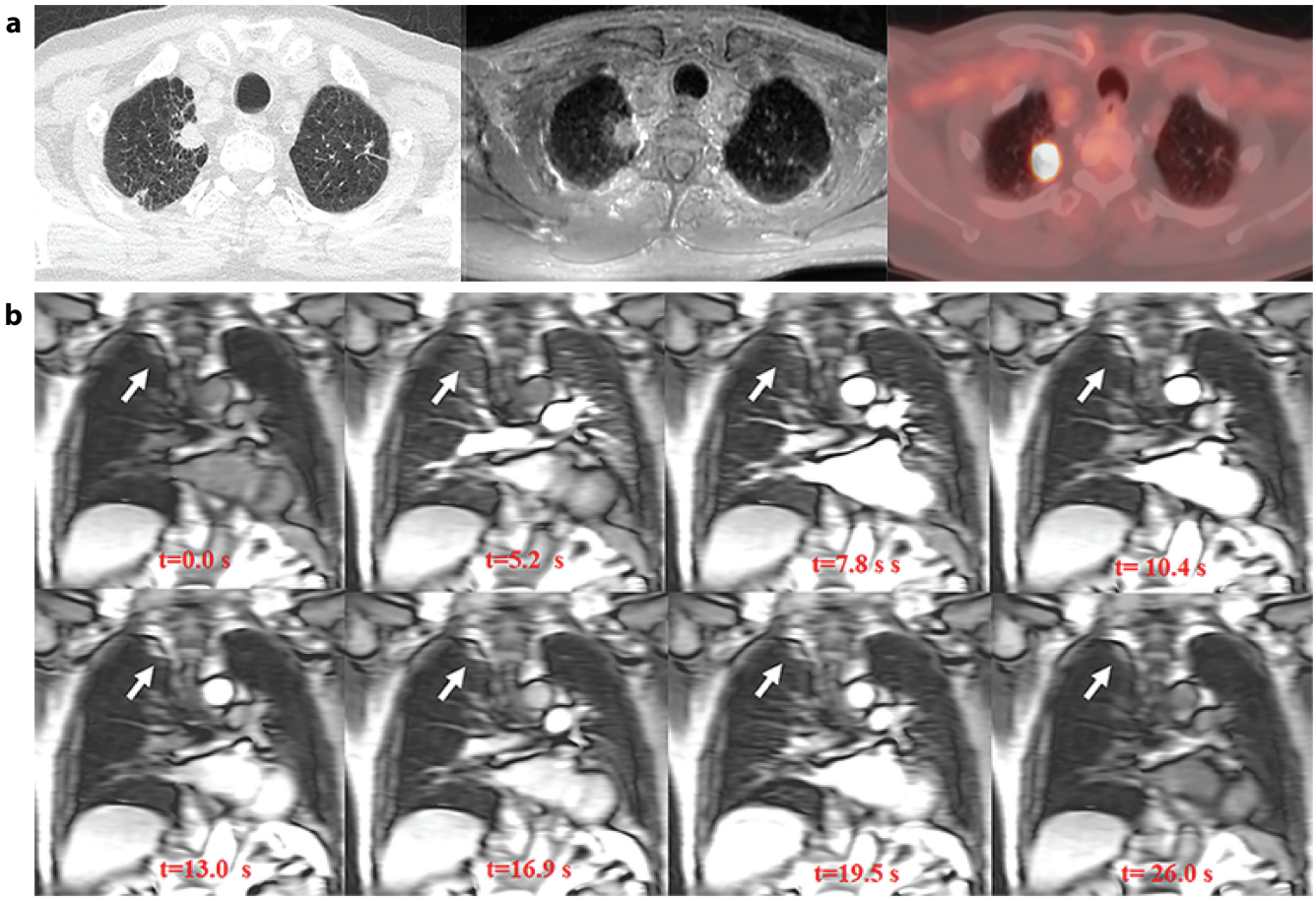

Fig. 4 Images in 82-year-old man with invasive adenocarcinoma in right upper lobe. **a**: Thin-section CT scan with 1-mm-thick sections (left), pulmonary MRI scan with ultrashort echo time at 110 msec and 1-mm-thick sections (middle), and fluorine 18 FDG PET/CT scan with 2.5-mm-thick sections (right). CT and MRI scans show solid nodule with notch. This nodule demonstrates high FDG uptake on PET/CT scan. CT and MRI scans also show bullae and emphysematous lung surrounding tumor. **b**: Dynamic first-pass contrast material-enhanced perfusion gradient-echo MRI scans obtained with a 3-T system demonstrate well-enhanced nodule (arrows) in right upper lobe. This nodule shows enhancement from lung parenchymal phase and is well enhanced at systemic circulation phase. t is the time after injection of gadolinium-based contrast agent followed by saline chaser. (Reproduced, with permission, from reference No. 2) FDG, fluorodeoxyglucose.

Mediastinal tumor characterization and TNM staging

For mediastinal tumor evaluations, CT is the first and most widely used modality for detection and diagnosis. However, as has been reported in the past literature, MR imaging provides important findings for disease diagnosis and facilitates accurate assessment of location, pattern of extension, and anatomical relationship with adjacent structures for various types of mediastinal tumors such as thymic epithelial tumor, mediastinal malignant lymphoma, germ cell tumor, teratoma, and cystic tumors, including bronchogenic cyst, thymic cyst, pericardial cyst, and neurogenic tumors.[18,107]

Since 2003, chemical shift MR imaging has been introduced as useful for differentiation of thymic hyperplasia from other thymic tumors. This MR technique can depict intravoxel fat and water within the tissue and has been frequently used for the adrenal gland and liver. Overall, chemical shift MR imaging can depict physiological fatty replacement of the normal thymus in nearly 50% of subjects age 11–15 years, and in nearly 100% of those over 15 years.[108] True thymic hyperplasia is defined as an increase in the size of thymus with the usual gross and histological appearance, and commonly occurs as a rebound phenomenon secondary to atrophy caused by chemotherapy.[109] On CT and MRI, thymic hyperplasia appears as an enlargement of the thymus, and its attenuation seen on CT and signal intensity on MRI are similar to those of the normal thymus.[107] In patients with enlarged thymus more than 15 years old, chemical shift MR imaging can diagnose thymic hyperplasia by detecting fatty infiltration within the thymus and has been recommended as useful for differentiation of thymic hyperplasia from other neoplastic processes.[110,111] Moreover, DWI has recently been used for mediastinal

Table 3 Diagnostic performance of dynamic contrast-enhanced MR imaging for distinguishing malignant from benign pulmonary nodules

	Year	Modality	Field strength (T)	MR sequence	Parameters	No. of nodule	SE (%)	SP (%)	AC (%)	
Hittmair K, et al.[77]	1995	Dynamic contrast-enhanced MR imaging	1.5	2D FLASH	Enhancement factor	20	100	67	91	
					Relative signal intensity increase		100	17	76	
Gückel C, et al.[78]	1996	Dynamic contrast-enhanced MR imaging	1.5	2D turbo FISP	Percentage increase in signal intensity	28	100	50	86	
					Enhancement curves		100	88	96	
Ohno Y, et al.[79]	2002	Dynamic first-pass contrast-enhanced MR imaging	1.5	3D radio-frequency spoiled GRE (i.e. 3D-fast field echo)	Mean maximum relative enhancement ratio	58	100	75	91	
					Slope of enhancement		100	85	95	
Schaefer JF, et al.[80]	2004	Dynamic contrast-enhanced MR imaging	1.5	2D T1-weighted in-phase GRE	Maximum peak	51	96	88	92	
					Slope		96	75	86	
					Washout		52	100	75	
Kono R, et al.[81]	2007	N/A	1.5	2D T1-weighted spin-echo	Maximum enhancement ratio	202	63	84	67	malignant nodule vs. OP
							81	81	81	malignant nodule vs. hamartoma
					Slope		55	71	58	malignant nodule vs. OP
							94	96	94	malignant nodule vs. hamartoma
					Washout ratio		83	63	80	
Ohno Y, et al.[82]	2008	Dynamic first-pass contrast-enhanced MR imaging	1.5	3D radio-frequency spoiled GRE (i.e. 3D-fast field echo)	Mean maximum relative enhancement ratio	202	96	54	86	
					Slope of enhancement		96	64	88	
		Dynamic contrast-enhanced MDCT	NA	NA	Maximum enhancement combined with absolute loss of enhancement		93	42	80.7	
					Net enhancement combined with absolute loss of enhancement		93	52	83.2	
					Slope of enhancement combined with absolute loss of enhancement		93	48	82	
		PET/CT	NA	N/A	SUV_{max}		93	54	84	
Zou Y, et al.[83]	2008	Dynamic contrast-enhanced MR imaging	1.5	T1-weighted fast spin-echo	Steepest slope in time–signal intensity	68	81	98	94	Benign SPN vs. malignant and active inflammatory SPN
					Enhancement of signal intensity at 4th min on time–signal intensity curve		93	100	94	Malignant SPN vs. active inflammatory SPN

(*Continued*)

Table 3 (Continued).

	Year	Modality	Field strength (T)	MR sequence	Parameters	No. of nodule	SE (%)	SP (%)	AC (%)
Coolen J, et al.[84]	2014	DWI	3	spin-echo type echo planar imaging	ADC_{high} (ADC determined from b values 500, 750 and 1,000 s/mm^2)	54	98	36	85
		Dynamic contrast-enhanced MR imaging		3D radio-frequency spoiled GRE (i.e. 3D-fast field echo)	Visual curve typing		100	51	91
		Dynamic contrast-enhanced MR imaging with DWI			Visual curve typing with ADC_{high} (ADC determined from b values 500, 750 and 1,000 s/mm^2)		98	82	94
		PET/CT	N/A	N/A	SUV contrast ratio		93	36	76
Ohno Y, et al.[85]	2015	Dynamic first-pass contrast-enhanced MR imaging	3	3D radio-frequency spoiled GRE (i.e. 3D-fast field echo)	Maximum relative enhancement ratio	218	92	49	76
					Slope of enhancement ratio		93	49	76
		Dynamic first-pass contrast-enhanced ADCT	NA	N/A	Total perfusion		92	71	84
					Pulmonary arterial perfusion		90	26	65
					Systemic arterial perfusion		89	26	65
					Nodule perfusion		91	28	67
		PET/CT	NA	N/A	SUV_{max}		89	31	67
Ohno Y, et al.[86]	2019	Dynamic first-pass contrast-enhanced ADCT	NA	N/A	Total perfusion	71	91	81	87
					Pulmonary arterial perfusion		84	77	82
					Systemic arterial perfusion		84	65	78
		Dynamic first-pass contrast-enhanced MR imaging	3	3D radio-frequency spoiled GRE (i.e. 3D-fast field echo)	Total perfusion		89	85	87
					Pulmonary arterial perfusion		84	77	82
					Systemic arterial perfusion		84	65	78
		PET/CT	NA	N/A	SUV_{max}		82	83	79

AC, accuracy; ADC, apparent diffusion coefficient; DWI, diffusion-weighted imaging; FISP, fast imaging with steady-state precession; FLASH, fast low-angle shot magnetic resonance imaging; GRE, gradient-echo; OP, organizing pneumonia; PET, positron emission tomography; SE, sensitivity; SP, specificity; SPN, solitary pulmonary nodule; SUV, standardized uptake value; SUV_{max}, maximum standardized uptake value.

evaluation in routine clinical practice. Seki et al. reported that quantitatively assessed DWI has a better capability than CT for the management of anterior mediastinal tumors and can play an important role in differentiating mediastinal tumors requiring further intervention or treatment from those requiring only follow-up examination or no further evaluation.[112] Dynamic CE-MR imaging has also been introduced as a tool equally as useful as DWI for mediastinal tumor assessment.[113] These techniques, as well as conventional T1-, T2-, and CE-T1-weighted imaging with fast or turbo SE imaging with and without fat suppression technique, are considered key participants in the diagnosis of mediastinal tumors in routine clinical practice. Moreover, whole-body MR imaging and FDG-PET/MRI, as well as FDG-PET/CT, showed better interobserver agreement and accuracy for evaluation of TNM stage in thymic epithelial tumors using the new the International Association for the Study of Lung Cancer (IASLC) and the International Thymic Malignancies Interest Group (ITMIG) thymic epithelial tumor staging than conventional imaging examinations consisting of CT, brain MR imaging, and bone scintigraphy.[62] Therefore, whole-body MR imaging may be considered as a one-stop shopping modality for TNM stage assessment as

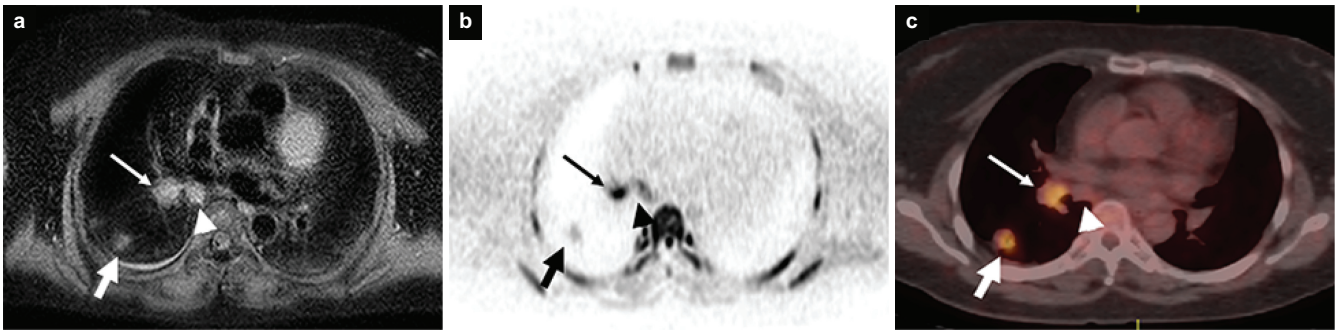

Fig. 5 Images in a 73-year-old patient with pathologically diagnosed N2 adenocarcinoma. **a**: STIR turbo SE image shows that primary lesion (medium arrow), subcarina lymph node (thick arrow), and right hilar lymph node (thin arrow) have high SI. Primary lesion in the right lower lobe is visible in the same axial plane. LSRs of lymph nodes were 0.75 (right hilar lymph node) and 0.78 (subcarina lymph node); LMRs were 1.7 (right hilar lymph node) and 1.9 (subcarina lymph node); and visual scores were 5. An accurate diagnosis of N2 disease was made. **b**: DW MR image shows that primary lesion (medium arrow), subcarina lymph node (thick arrow), and right hilar lymph node (thin arrow) have high SI. Primary lesion in the right lower lobe is visible in the same axial plane. ADCs of lymph nodes were 2.8×10^{-3}sec/mm^2 (right hilar lymph node) and 3.4×10^{-3}sec/mm^2(subcarina lymph node), and visual scores were 5. An accurate diagnosis of N2 disease was made. **c**: FDG PET/CT image shows that primary lesion (medium arrow) and right hilar lymph node (thin arrow) have high uptake of FDG, and subcarina lymph node (thick arrow) has low uptake of FDG. Primary lesion in the right lower lobe is visible in the same axial plane. SUV_{max} of lymph nodes was 3.2 (right hilar lymph node) and 1.5 (subcarina lymph node), and visual scores were 5 (right hilar lymph node) and 2 (subcarina lymph node). An inaccurate diagnosis of N1 was made. (Reproduced, with permission, from reference No. 99) ADC, apparent diffusion coefficient; DW, diffusion-weighted; FDG, fluorodeoxyglucose; LMR, lymph node-to-muscle ratio; LSR, lesion-to-saline ratio; PET, positron emission tomography; SE, spin-echo; SI, signal intensity; STIR, short inversion time inversion recovery; SUV_{max}, maximum standardized uptake value.

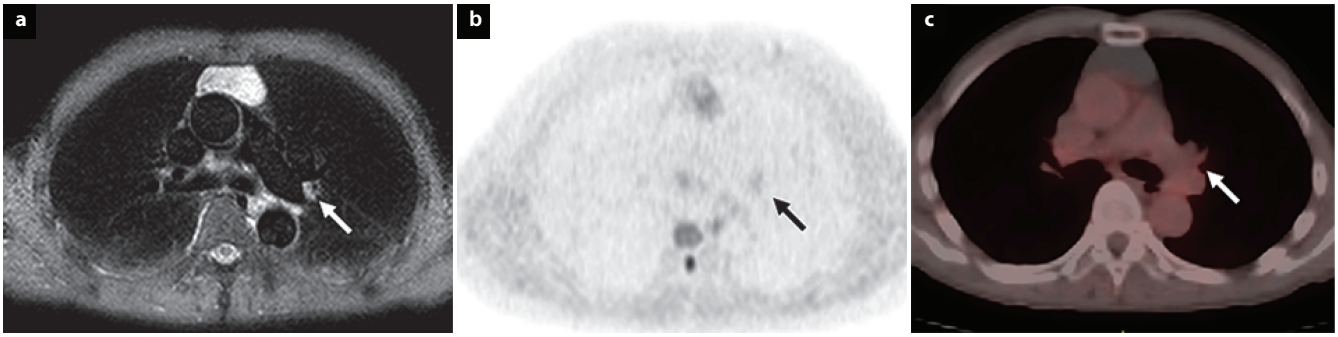

Fig. 6 Images in a 72-year-old patient with pathologically diagnosed N1 adenocarcinoma. **a**: STIR turbo SE image shows that left hilar lymph node (arrow) has high SI. Primary lesion is not visible in the same axial plane. Thymic cyst can be seen in the anterior mediastinum. LSR of the lymph node was 0.70, LMR was 1.5, and visual score was 5. An accurate diagnosis of N1 disease was made. **b**: DW MR image shows that left hilar lymph node (arrow) has low SI. Primary lesion is not visible in the same axial plane. Thymic cyst can be seen as low SI in anterior mediastinum. ADC of the lymph node was 1.5×10^{-3}sec/mm^2, and visual score was 2. An inaccurate diagnosis of N0 was made. **c**: FDG PET/CT image shows that left hilar lymph node (arrow) has low uptake of FDG. Primary lesion is not visible in the same axial plane. Thymic cyst can be seen in the anterior mediastinum. SUV_{max} of the lymph node was 1.2, and visual score was 1. An inaccurate diagnosis of N0 disease was made. (Reproduced, with permission, from reference No. 99) ADC, apparent diffusion coefficient; DW, diffusion-weighted; FDG, fluorodeoxyglucose; LMR, lymph node-to-muscle ratio; LSR, lesion-to-spinal cord ratio; PET, positron emission tomography; SE, spin-echo; SI, signal intensity; STIR, short inversion time inversion recovery; $SUV_{max,}$ maximum standardized uptake value.

well as mediastinal tumor evaluation as a complement for conventional radiological examinations in routine clinical practice.

Malignant mesothelioma evaluation

Pleural malignancy is usually first suspected on the basis of clinical history and chest radiographs, with further assessment by CT or MRI, and FDG-PET/CT if required. Currently, CT is usually the preferred initial investigation for pleural disease. Although MR imaging is not commonly the first-line modality for imaging of suspected pleural malignancy, it may be useful in difficult cases or for patients with a contraindication of iodinated contrast medium. Falaschi et al. compared the diagnostic accuracy of MR and CT for patients with pleural disease and found that the two methods were equally good for assessing morphological features.[114]

Table 4 Diagnostic performance of T factor evaluation with MR imaging

Author	Year	Field strength (T)	Sequence	MR imaging			CT			Standard reference
				SE (%)	SP (%)	AC (%)	SE (%)	SP (%)	AC (%)	
Webb, et al.[1]	1991	0.35 or 1.5	ECG-gated T1- and T2-weighted spin-echo	80	56	73	84	63	78	Surgical and pathological diagnosis
Sakai, et al.[88]	1997	1.5	Free-breathing Cine-GRASS	10	70	76	80	65	68	Surgical and pathological diagnosis
Ohno, et al.[89]	2001	1.5	dynamic ECG-triggered 3D-GRE	78-90	73-87	75-88	67-70	60-64	68-71	Surgical and pathological diagnosis
Tang, et al.[90]	2015	3	Breath-hold dynamic CE 2D-GRE	N/A	N/A	82.2	N/A	N/A	84.4	Pathological diagnosis

AC, accuracy; CE, contrast enhanced; ECG, electrocardiogram; GRASS, gradient recalled acquisition in the steady state; GRE, gradient echo; SE, sensitivity; SP, specificity.

Table 5 Diagnostic performance of N factor evaluation with MR imaging

Author	Year	Field strength (T)	Sequence	MR imaging			CT			FDG-PET/CT			Analysis
				SE (%)	SP (%)	AC (%)	SE (%)	SP (%)	AC (%)	SE (%)	SP (%)	AC (%)	
Takenaka, et al.[91]	2002	1.5	ECG-triggered T1W TSE, STIR	52 or 100	91 or 96	83or 96	52	91	83	N/A	N/A	N/A	per-node basis
Ohno, et al.[92]	2004	1.5	STIR	93	87	89	53	83	72	N/A	N/A	N/A	per-node basis and per-patient basis
Ohno, et al.[93]	2007	1.5	STIR	84 or 90	74 or 77	88 or 92	88	90 or 93	82.6	N/A	N/A	N/A	per-node basis and per-patient basis
Hasegawa, et al.[94]	2008	1.5	DWI (b = 0 and 1000 s/mm^2) by SS-SE-EPI	80	97	95	N/A	N/A	N/A	N/A	N/A	N/A	per-patient basis
Nomori, et al.[95]	2008	1.5	DWI (b = 0 and 1000 s/mm^2) by SS-SE-EPI	67	99	98	N/A	N/A	N/A	72	97	96	per-node basis and per-patient basis
Morikawa, et al.[96]	2009	1.5	STIR	93.9 or 96.3	67.3 or 70.9	84.7	N/A	N/A	N/A	90.2	65.5	80.3	per-node basis and per-patient basis
Nakayama, et al.[97]	2010	1.5	DWI (b = 50 and 1000 s/mm^2) by SS-SE-EPI	69	100	94	N/A	N/A	N/A	N/A	N/A	N/A	per-node basis and per-patient basis
Usuda, et al.[98]	2011	1.5	T1W SE, T2W FSE and DWI (b = 0 and 800 s/mm^2) by SS-SE-EPI	59	93	81	N/A	N/A	N/A	33	90	71	per-node basis and per-patient basis
Ohno, et al.[99]	2011	1.5	STIR, DWI (b = 0 and 1000 s/mm^2) by SS-SE-EPI	71.0 or 82.8	88.5 or 90.4	82.8 or 86.8	N/A	N/A	N/A	69.9 or 74.2	91.7 or 92.4	83.6 or 85.6	per-node basis and per-patient basis
Ohno, et al.[100]	2015	3	STIR-FASE, DWI (b = 0 and 300 s/mm^2) by SS-SE-EPI and FASE	60.3–82.1	98.7	79.5–90.4	N/A	N/A	N/A	57.7	97.4	77.6	per-node basis and per-patient basis
Usuda, et al.[101]	2015	1.5	T1W SE, T2W FSE, DWI (b = 0 and 800 s/mm$_2$) by SS-SE-EPI	71	100	91	N/A	N/A	N/A	86	31	48	per-patient basis
Nomori, et al.[102]	2016	1.5	DWI (b = 800 s/mm^2) by SS-SE-EPI	38 or 79	92 or 94	75	N/A	N/A	N/A	33 or 58	89 or 90	67	per-node basis and per-patient basis
Peerlings, et al.[103]	2016	Mainly 1.5T (Meta-Analysis)	DWI and STIR	86.5	88.2	N/A	N/A	N/A	N/A	N/A	N/A	N/A	per-node basis and per-patient basis

AC, accuracy; DWI, diffusion-weighted imaging; ECG, electrocardiogram; FASE, fast advanced spin-echo; FSE, fast spin-echo; SE, sensitivity; SP, specificity; SS-SE-EPI, single shot spin-echo type echo planar imaging; T1W, T1-weighted; T2W, T2-weighted; TSE, turbo spin-echo.

Table 6 Diagnostic performance of M factor evaluation with MR imaging

Author	Year	Field strength (T)	Whole-body MRI			FDG-PET/MRI			FDG-PET/CT		
			SE (%)	SP (%)	AC (%)	SE (%)	SP (%)	AC (%)	SE (%)	SP (%)	AC (%)
Ohno, et al.[54]	2007	1.5	N/A	N/A	80	N/A	N/A	N/A	N/A	N/A	73.3
Yi, et al.[55]	2008	3	N/A	N/A	86	N/A	N/A	N/A	N/A	N/A	86
Ohno, et al.[56]	2008	1.5	58 or 70	88 or 92	82 or 88	N/A	N/A	N/A	63	95	88
Takenaka, et al.[57]	2009	1.5	73 or 96	94 or 96	94 or 96	N/A	N/A	N/A	97	96	96
Ohno, et al.[60]	2015	3	100	88	99	93 or 100	81 or 88	91 or 99	93	75	91
Lee, et al.[106]	2016	3	N/A	N/A	N/A	83	100	98	67	100	96
Ohno Y, et al.[64]	2020	3	N/A	N/A	94 or 97	N/A	N/A	94 or 97	N/A	N/A	96

Standard reference for M-stage in each study was determined by standard imaging, pathological examination and follow-up examination results. AC, accuracy; FDG, fluorodeoxyglucose; PET, positron emission tomography; SE, sensitivity; SP, specificity.

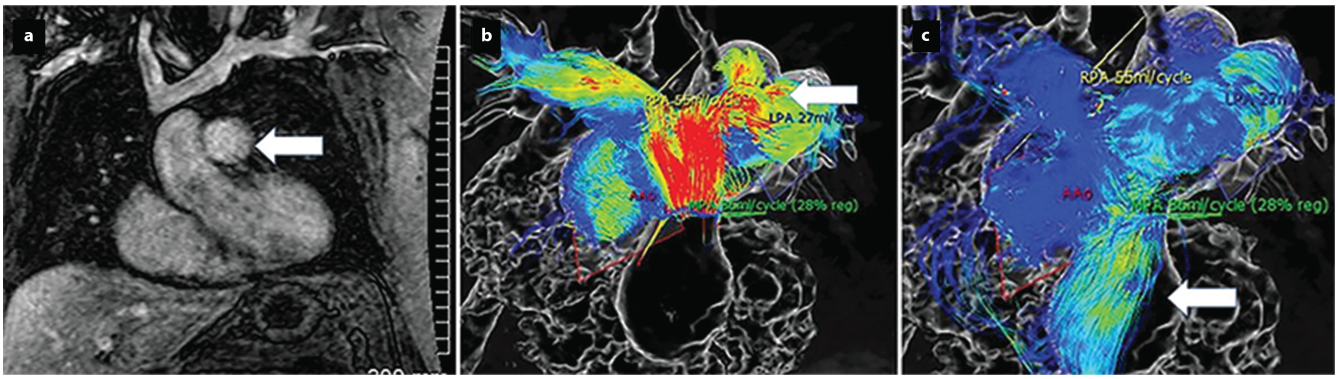

Fig. 7 Images in 42-year-old woman with chronic pulmonary arterial hypertension from an atrial septal defect with pulmonary insufficiency. **a**: Coronal MR angiogram shows an enlarged pulmonary artery (arrow). **b**: Four-dimensional flow systolic phase path lines from emitter plane at pulmonary valve show rapid flow in red at the pulmonary trunk and turbulent (helical) flows in right and left (arrow) pulmonary arteries. **c**: Four-dimensional flow in diastolic phase shows lower velocity pulmonary insufficiency path lines in blue (arrow) from same emitter plane at pulmonary valve, with calculated regurgitant fraction of 28%. (Reproduced, with permission, from reference No. 2)

There are several types of malignant pleural tumors with several causes, and malignant pleural mesothelioma (MPM) is one of the most aggressive malignant neoplasms, with epithelial, sarcomatoid, and mixed as its major histologic subtypes. While osteosarcomatous degeneration within MPM is considered a rare subtype, the majority of MPM cases are associated with asbestos exposure. In fact, although MPM was once uncommon, its incidence is increasing worldwide as a result of widespread exposure to asbestos.[115,116]

MR imaging is superior to CT for the differentiation of malignant from benign pleural disease.[114–118] In addition, MR imaging using various sequences with and without contrast media has been found to be useful for evaluation of tumor extent in MPM patients.[119,120] MPM is generally divided into three histologic subtypes: epithelioid, sarcomatoid, and biphasic, with a significant difference in prognosis between epithelioid and nonepithelioid (biphasic and sarcomatoid) MPM.[121] A study demonstrated that quantitatively assessed DWIs show a significant difference in the ADC between the epithelioid and sarcomatoid subtypes, suggesting that DWI is capable of MPM evaluation, especially subtype assessment in routine clinical practice.[122] A few studies of evaluation of the TNM stage in MPM demonstrated that the capability of whole-body MR imaging or FDG-PET/MRI was superior to that of FDG-PET/CT or conventional radiological examination.[63,123] Although the disease frequency of MPM is quite low and gathering more evidence may thus be difficult, whole-body MR imaging as well as dedicated thoracic MR imaging may perform a complementary function for management of MPM in routine clinical practice.

Pulmonary hypertension

Pulmonary hypertension (PH) is defined as a mean pressure of > 20 mmHg in the main pulmonary artery at rest in the supine position measured by means of right heart

catheterization.[124,125] Pulmonary arterial hypertension (PAH) characterizes a very specific group of PH patients defined by a pulmonary capillary wedge pressure of < 15 mm Hg and a pulmonary vascular resistance of > 3 Wood units in the absence of lung disease or chronic thromboembolic pulmonary hypertension (CTEPH).[124] The reader is referred to the recent consensus statement by the European Society of Cardiology and European Respiratory Society (ESC/ERS) guidelines for an excellent overview of the diagnosis and treatment of this disorder.[126,127] The diagnostic paradigm currently includes ventilation perfusion (V/Q) SPECT lung scanning for CTEPH evaluation. In addition, dynamic CE-perfusion MR imaging has been shown to have equal sensitivity and specificity to those of both planar scintigraphy and SPECT for CTEPH screening.[128,129] Furthermore, cardiovascular MR imaging has been strongly recommended for aspects of patient management such as the initial diagnosis, follow-up, and therapeutic effect evaluation (Fig. 7).[130,131] Findings of septal flattening, delayed contrast enhancement of the septal insertions, and an elevation in the right ventricular end diastolic volume index (RVEDVI) are of prognostic value for PH.[132–135] In addition, quantitatively assessed CE-MR angiography is useful for the assessment of the severity of PH and the longitudinal assessment of therapy effect.[136–139] CE-MR angiography has been used for CTEPH to diagnose proximal arterial enlargement, webs of chronic thrombi, and amputation of the smaller pulmonary arterial branches. Bright-blood steady state free precession imaging can also be used to delineate thrombi in the major pulmonary vessels in patients with CTEPH[140] and reveal a reduced flow in the pulmonary artery due to PH.[141] Distensibility in the pulmonary artery is also predictive of outcomes for patients with PH,[140,142] while RVEDVindex and PA area can also predict survival,[143] with all of the validity of these aspects confirmed via meta-analysis.[144] In addition, right ventricular evaluation using cardiovascular MR imaging was suggested as a useful procedure for characterization and disease severity evaluation of pulmonary hypertension.[145–147] Therefore, strong evidence supports the current clinical use of cardiopulmonary MR imaging for PH patients. Table 7 shows major study results for assessment of pulmonary hypertension by means of cardiac MR imaging.

Pulmonary thromboembolism

Pulmonary thromboembolism (PTE) is a common disorder that is part of the spectrum of venous thromboembolic diseases. PTE can have a high mortality if not diagnosed; however, even the most common treatment for this disorder carries a risk of significant morbidity and mortality, particularly for the aged. In routine clinical practice, diagnostic testing for PE is vital and CE-CT angiography (CTA) has become the test of choice. Currently, the CTA positivity rates for PE are lower than 10% at most medical centers, and overtesting is now an issue along with overdiagnosis for PTE.[148,149]

Since 2004, Time-resolved or 4D CE-MR angiography has improved the spatial and temporal resolution of CE-MR angiography with parallel imaging techniques and has revealed both the direct signs of PTE within pulmonary arteries and lung perfusion.[150–152] This technique can be considered an alternative to CT angiography for patients presenting with signs and symptoms of PTE, and may be at least as effective as pulmonary digital subtraction angiography.[2,150–156] In addition, the investigators involved in the PIOPED III study reported a very high percentage of technically inadequate examinations (mean, 25%), with as many as 52% of examinations at individual centers found to fall within that category. These findings give rise to further questions, such as whether all participating centers had extensive experience with CE-MR angiography, since at the time of the study, even the PIOPED III study did not use time-resolved CE-MR angiography, which is easier to use in routine clinical practice. In addition, PTE was correctly diagnosed in only 57% of patients by the centers enrolled in this study which used technically inadequate examinations. However, if only the results obtained with technically adequate examinations were taken into consideration, non-time-resolved CE-MR angiography showed a sensitivity of 78%. The investigators, therefore, concluded that the use of non-time-resolved CE-MR angiography should be considered only at the centers that routinely perform CE-MR angiography well and only for patients for whom standard tests are contraindicated.[156] The main results of this study are listed in Table 8. These results indicate that CE-MR angiography can be used in routine clinical practice as a substitute or in a complementary role for CE-CT angiography in the management of PTE patients.

Future Directions and Conclusion

Until recently, the clinical uses of MR imaging for thoracic diseases have been limited; however, recently developed methods are now providing more opportunities to exploit the advantages of MR imaging for the evaluation of many common lung disorders. State-of-the-art MR imaging can non-invasively visualize lung structural and functional abnormalities without ionizing radiation, and thus provide an alternative to CT. Major efforts must, therefore, be made by vendors and developers to maximize the potential of MR imaging for improving care of patients with thoracic diseases to ensure that novel pulse sequences and measurements be made available more widely and more quickly. While CT will remain the principal imaging tool for routine pulmonary imaging examinations in thoracic diseases, MR imaging is emerging as the clinical standard or at least shows great

Table 7 Cardiovascular magnetic resonance biomarkers for assessment of pulmonary hypertension

Author	Year	No. of patients	Field strength (T)	Cardiac MR indexes	Hazard Ratio		Hazard Ratio 95% C.I.	*P* value
Gan, et al.[142]	2007	70	1.5	PA RAC	0.87	(risk of mortality)	0.79-0.96	0.006
van Wolferen, et al.[132]	2007	64	1.5	SVI	0.764	(risk of mortality)	N/A	< 0.001
				RVEDVI	1.61			< 0.001
				LVEDVI	0.705			0.002
van de Veerdonk, et al.[134]	2011	110	1.5	RVESVI	1.014	(risk of mortality)	1.001-1.027	0.048
				RVEF	0.938		0.902-0.975	0.001
				LVEDVI	0.962		0.931-0.994	0.019
				LVESVI	0.942		0.888-0.998	0.045
				SVI	0.945		0.899-0.993	0.025
Swift, et al.[131]	2014	79	1.5	FWHM	1.08	(risk of mortality)	1.01-1.16	0.034
				PTT	1.1		1.03-1.18	0.01
Baggen, et al.[144]	2016	539	N/A (meta-analysis)	RVEF	1.23	(prognostic value)	1.07-1.41	0.003
				RVEDVI	1.06		1.00-1.12	0.049
				RVESVI	1.05		1.01-1.09	0.013
				LVEDVI	1.16		1.00-1.34	0.045
de Siqueira, et al.[145]	2016	110	1.5	GLS	1.06	(risk of disease severity, associated with clinically relevant outcomes)	1-1.12	0.026
				RVEF	0.97		0.94-0.99	0.03
				GLSR	2.52		1.03-6.1	0.04
				GCSR	4.5		1.3-15.6	0.01
Swift, et al.[143]	2017	576	1.5	RVESV	1.217	(risk of mortality)	1.061-1.539	0.005
				PA RAC	0.762		0.623-0.932	0.008

C.I., confidence interval; FWHM, full width at half maximum; GCSR, global circumferential strain rate; GLS, global longitudinal strain; GLSR, global longitudinal strain rate; LVEDVI, left ventricular end-diastolic volume index; LVESVI, left ventricular end-systolic volume index; PA RAC, pulmonary artery relative area change; PTT, pulmonary transit time; RVEDVI, right ventricular end-diastolic volume index; RVEF, right ventricular ejection fraction; RVESV, right ventricular end-diastolic volume; RVESVI, right ventricular end-systolic volume index; SVI, stroke volume index.

potential for changing clinical care for certain patients and indications. In addition, MR imaging is considered as a tool that can provide unique information of clinical interest and can be utilized for physiologic, pathophysiologic, and hypothesis-driven research and preclinical studies of various thoracic diseases. Finally, prospective, randomized, and multi-center trials need to be conducted to directly compare MR imaging with conventional clinical methods to determine whether the former is of equal or superior clinical relevance for many thoracic diseases. The results of these trials together with continued improvements can be expected to result in further updates or modifications of recommendations for the use of MR imaging.

Acknowledgments

The authors thank Canon Medical Systems Corporation, Daiichi-Sankyo, Co., Ltd., or Bayer Yakuhin, Ltd. for their financial support for Drs. Ohno, Murayama, Yoshikawa, and Toyama.

Conflicts of Interest

Drs. Ohno, Murayama, Yoshikawa, and Toyama received research grants from Canon Medical Systems Corporation, Daiichi-Sankyo, Co., Ltd., or Bayer Yakuhin, Ltd. The other authors have no conflict of interest.

Table 8 Major study results for demonstrating diagnostic performance of non-time-resolved and time-resolved CE-MR angiography for patients undergoing PTE screening on a per-patient basis

Authors	Year	No. of patients	Field strength (T)	Method(s)	Gold standard	SE (%)	SP (%)
Meaney, et al.[153]	1997	30	1.5	Non-time-resolved 3D CE-MR angiography	Pulmonary DSA	75-100	95-100
Gupta, et al.[154]	1999	36	1.5	Non-time-resolved 3D CE-MR angiography	Pulmonary DSA	85	96
Oudkerk, et al.[155]	2002	141	1.5	Non-time-resolved 3D CE-MR angiography	Pulmonary DSA	77	98
Ohno et al.[151]	2004	48	1.5	Time-resolved 3D CE-MR angiography	Pulmonary DSA	92	94
Kluge, et al.[152]	2006	62	1.5	Real-time MR imaging used True FISP, non-time-resolved 3D CE-MR angiography and dynamic 3D CE-perfusion MR imaging	16-detector row CT angiography	81	100
Stein, et al.[156]	2010	371	1.5 and 3	3D CE-MR angiography	Combination of various tests	78	99

CE, contrast enhanced; FISP, fast imaging with steady-state precession; PTE, pulmonary thromboembolism; SE, sensitivity; SP, specificity.

Supplement Materials

SI. Promising Developments Requiring Further Validation or Evaluation

SII. Developments Warranting Research Investigations in Preclinical or Patient Studies

References

1. Webb WR, Gatsonis C, Zerhouni EA, et al. CT and MR imaging in staging non-small cell bronchogenic carcinoma: report of the Radiologic Diagnostic Oncology Group. Radiology 1991; 178:705–713.
2. Hatabu H, Ohno Y, Gefter WB, et al.; Fleischner society. Expanding applications of pulmonary MRI in the clinical evaluation of lung disorders: Fleischner society position paper. Radiology 2020; 297:286–301.
3. Schiebler ML, Parraga G, Gefter WB, et al. Synopsis from expanding applications of pulmonary MRI in the clinical evaluation of lung disorders: Fleischner society position paper. Chest 2021; 159:492–495.
4. Mayo JR. Thoracic magnetic resonance imaging: physics and pulse sequences. J Thorac Imaging 1993; 8:1–11.
5. Kono M, Adachi S, Kusumoto M, et al. Clinical utility of Gd-DTPA-enhanced magnetic resonance imaging in lung cancer. J Thorac Imaging 1993; 8:18–26.
6. Kauczor HU, Kreitner KF. MRI of the pulmonary parenchyma. Eur Radiol 1999; 9:1755–1764.
7. Hatabu H, Chen Q, Stock KW, et al. Fast magnetic resonance imaging of the lung. Eur J Radiol 1999; 29:114–132.
8. Mayo JR. MR imaging of pulmonary parenchyma. Magn Reson Imaging Clin N Am 2000; 8:105–123.
9. Ohno Y, Chen Q, Hatabu H. Oxygen-enhanced magnetic resonance ventilation imaging of lung. Eur J Radiol 2001; 37:164–171.
10. Salerno M, Altes TA, Mugler JP, et al. Hyperpolarized noble gas MR imaging of the lung: potential clinical applications. Eur J Radiol 2001; 40:33–44.
11. Ohno Y, Sugimura K, Hatabu H. MR imaging of lung cancer. Eur J Radiol 2002; 44:172–181.
12. Ohno Y, Sugimura K, Hatabu H. Clinical oxygen-enhanced magnetic resonance imaging of the lung. Top Magn Reson Imaging 2003; 14:237–243.
13. Fain SB, Korosec FR, Holmes JH, et al. Functional lung imaging using hyperpolarized gas MRI. J Magn Reson Imaging 2007; 25:910–923.
14. Sieren JC, Ohno Y, Koyama H, et al. Recent technological and application developments in computed tomography and magnetic resonance imaging for improved pulmonary nodule detection and lung cancer staging. J Magn Reson Imaging 2010; 32:1353–1369.
15. Ohno Y, Koyama H, Yoshikawa T, et al. Pulmonary magnetic resonance imaging for airway diseases. J Thorac Imaging 2011; 26:301–316.
16. Koyama H, Ohno Y, Seki S, et al. Magnetic resonance imaging for lung cancer. J Thorac Imaging 2013; 28:138–150.
17. Liszewski MC, Hersman FW, Altes TA, et al. Magnetic resonance imaging of pediatric lung parenchyma, airways, vasculature, ventilation, and perfusion: state of the art. Radiol Clin North Am 2013; 51:555–582.
18. Ohno Y. New applications of magnetic resonance imaging for thoracic oncology. Semin Respir Crit Care Med 2014; 35:27–40.
19. Ohno Y, Nishio M, Koyama H, et al. Dynamic contrast-enhanced CT and MRI for pulmonary nodule assessment. AJR Am J Roentgenol 2014; 202:515–529.

20. Kim HS, Lee KS, Ohno Y, et al. PET/CT versus MRI for diagnosis, staging, and follow-up of lung cancer. J Magn Reson Imaging 2015; 42:247–260.
21. Ohno Y, Koyama H, Yoshikawa T, et al. Lung cancer assessment using MR imaging: an update. Magn Reson Imaging Clin N Am 2015; 23:231–244.
22. Kruger SJ, Nagle SK, Couch MJ, et al. Functional imaging of the lungs with gas agents. J Magn Reson Imaging 2016; 43:295–315.
23. Ohno Y, Koyama H, Yoshikawa T, et al. State-of-the-Art Imaging of the Lung for Connective Tissue Disease (CTD). Curr Rheumatol Rep 2015; 17:69.
24. Ohno Y, Koyama H, Lee HY, et al. Magnetic Resonance Imaging (MRI) and Positron Emission Tomography (PET)/MRI for lung cancer staging. J Thorac Imaging 2016; 31:215–227.
25. Ohno Y, Koyama H, Lee HY, et al. Contrast-enhanced CT- and MRI-based perfusion assessment for pulmonary diseases: basics and clinical applications. Diagn Interv Radiol 2016; 22:407–421.
26. Biederer J, Ohno Y, Hatabu H, et al. Screening for lung cancer: Does MRI have a role? Eur J Radiol 2017; 86:353–360.
27. Johns CS, Swift AJ, Hughes PJC, et al. Pulmonary MR angiography and perfusion imaging-A review of methods and applications. Eur J Radiol 2017; 86:361–370.
28. Ohno Y, Yoshikawa T, Kishida Y, et al. Unenhanced and contrast-enhanced MR angiography and perfusion imaging for suspected pulmonary thromboembolism. AJR Am J Roentgenol 2017; 208:517–530.
29. Ohno Y, Kauczor HU, Hatabu H, et al.; International Workshop for Pulmonary Functional Imaging (IWPFI). MRI for solitary pulmonary nodule and mass assessment: Current state of the art. J Magn Reson Imaging 2018; 47:1437–1458.
30. Ciliberto M, Kishida Y, Seki S, et al.. Update of MR Imaging for Evaluation of Lung Cancer. Radiol Clin North Am 2018; 56:437–469.
31. Tsuchiya N, van Beek EJ, Ohno Y, et al. Magnetic resonance angiography for the primary diagnosis of pulmonary embolism: A review from the international workshop for pulmonary functional imaging. World J Radiol 2018; 10:52–64.
32. Wielpütz MO, Triphan SMF, Ohno Y, et al. Outracing lung signal decay – potential of ultrashort echo time MRI. Rofo 2019; 191:415–423.
33. Cutillo AG, Morris AH, Blatter DD, et al. Determination of lung water content and distribution by nuclear magnetic resonance. J Appl Physiol Respir Environ Exerc Physiol 1984; 57:583–588.
34. Cutillo AG, Morris AH, Ailion DC, et al. Determination of lung water content and distribution by nuclear magnetic resonance imaging. J Thorac Imaging 1986; 1:39–51.
35. Cutillo AG, Ganesan K, Ailion DC, et al. Alveolar air-tissue interface and nuclear magnetic resonance behavior of lung. J Appl Physiol (1985) 1991; 70:2145–2154.
36. Mayo JR, MacKay A, Müller NL. MR imaging of the lungs: value of short TE spin-echo pulse sequences. AJR Am J Roentgenol 1992; 159:951–956.
37. Alsop DC, Hatabu H, Bonnet M, et al. Multi-slice, breath-hold imaging of the lung with submillisecond echo times. Magn Reson Med 1995; 33:678–682.
38. Hatabu H, Gaa J, Tadamura E, et al. MR imaging of pulmonary parenchyma with a half-Fourier single-shot turbo spin-echo (HASTE) sequence. Eur J Radiol 1999; 29:152–159.
39. Hatabu H, Alsop DC, Listerud J, et al. T2* and proton density measurement of normal human lung parenchyma using submillisecond echo time gradient echo magnetic resonance imaging. Eur J Radiol 1999; 29:245–252.
40. Ohno Y, Oshio K, Uematsu H, et al. Single-shot half-Fourier RARE sequence with ultra-short inter-echo spacing for lung imaging. J Magn Reson Imaging 2004; 20:336–339.
41. Takahara T, Imai Y, Yamashita T, et al. Diffusion weighted whole body imaging with background body signal suppression (DWIBS): technical improvement using free breathing, STIR and high resolution 3D display. Radiat Med 2004; 22:275–282.
42. Lenz C, Klarhöfer M, Scheffler K, et al. Assessing extracranial tumors using diffusion-weighted whole-body MRI. Z Med Phys 2011; 21:79–90.
43. Gibiino F, Sacolick L, Menini A, et al. Free-breathing, zero-TE MR lung imaging. MAGMA 2015; 28:207–215.
44. Ohno Y, Koyama H, Yoshikawa T, et al. Pulmonary high-resolution ultrashort TE MR imaging: Comparison with thin-section standard- and low-dose computed tomography for the assessment of pulmonary parenchyma diseases. J Magn Reson Imaging 2016; 43:512–532.
45. Ohno Y, Koyama H, Yoshikawa T, et al. Standard-, reduced-, and no-dose thin-section radiologic examinations: comparison of capability for nodule detection and nodule type assessment in patients suspected of having pulmonary nodules. Radiology 2017; 284:562–573.
46. Wielpütz MO, Lee HY, Koyama H, et al. Morphologic characterization of pulmonary nodules with ultrashort TE MRI at 3T. AJR Am J Roentgenol 2018; 210:1216–1225.
47. Ohno Y, Yui M, Chen Y, et al. Gadolinium-based blood volume mapping from MRI with ultrashort TE versus CT and SPECT for predicting postoperative lung function in patients with non-small cell lung cancer. AJR Am J Roentgenol 2019; 212:57–66.
48. Zeng F, Nogami M, Ueno YR, et al. Diagnostic performance of zero-TE lung MR imaging in FDG PET/MRI for pulmonary malignancies. Eur Radiol 2020; 30:4995–5003.
49. Takahashi M, Togao O, Obara M, et al. Ultra-short echo time (UTE) MR imaging of the lung: comparison between normal and emphysematous lungs in mutant mice. J Magn Reson Imaging 2010; 32:326–333.
50. Togao O, Ohno Y, Dimitrov I, et al. Ventilation/perfusion imaging of the lung using ultra-short echo time (UTE) MRI in an animal model of pulmonary embolism. J Magn Reson Imaging 2011; 34:539–546.
51. Ohno Y, Koyama H, Yoshikawa T, et al. T2* measurements of 3-T MRI with ultrashort TEs: capabilities of pulmonary function assessment and clinical stage classification in smokers. AJR Am J Roentgenol 2011; 197:W279–285.
52. Ohno Y, Nishio M, Koyama H, et al. Pulmonary MR imaging with ultra-short TEs: utility for disease severity

assessment of connective tissue disease patients. Eur J Radiol 2013; 82:1359–1365.
53. Ohno Y, Nishio M, Koyama H, et al. Pulmonary 3 T MRI with ultrashort TEs: influence of ultrashort echo time interval on pulmonary functional and clinical stage assessments of smokers. J Magn Reson Imaging 2014; 39:988–997.
54. Ohno Y, Koyama H, Nogami M, et al. Whole-body MR imaging vs. FDG-PET: comparison of accuracy of M-stage diagnosis for lung cancer patients. J Magn Reson Imaging 2007; 26:498–509.
55. Yi CA, Shin KM, Lee KS, et al. Non-small cell lung cancer staging: efficacy comparison of integrated PET/CT versus 3.0-T whole-body MR imaging. Radiology 2008; 248: 632–642.
56. Ohno Y, Koyama H, Onishi Y, et al. Non-small cell lung cancer: whole-body MR examination for M-stage assessment—utility for whole-body diffusion-weighted imaging compared with integrated FDG PET/CT. Radiology 2008; 248:643–654.
57. Takenaka D, Ohno Y, Matsumoto K, et al. Detection of bone metastases in non-small cell lung cancer patients: comparison of whole-body diffusion-weighted imaging (DWI), whole-body MR imaging without and with DWI, whole-body FDG-PET/CT, and bone scintigraphy. J Magn Reson Imaging 2009; 30:298–308.
58. Ohno Y, Nishio M, Koyama H, et al. Comparison of the utility of whole-body MRI with and without contrast-enhanced Quick 3D and double RF fat suppression techniques, conventional whole-body MRI, PET/CT and conventional examination for assessment of recurrence in NSCLC patients. Eur J Radiol 2013; 82:2018–2027.
59. Yi CA, Lee KS, Lee HY, et al. Coregistered whole body magnetic resonance imaging-positron emission tomography (MRI-PET) versus PET-computed tomography plus brain MRI in staging resectable lung cancer: comparisons of clinical effectiveness in a randomized trial. Cancer 2013; 119:1784–1791.
60. Ohno Y, Koyama H, Yoshikawa T, et al. Three-way comparison of whole-body MR, Coregistered whole-body FDG PET/MR, and integrated whole-body FDG PET/CT imaging: TNM and stage assessment capability for non-small cell lung cancer patients. Radiology 2015; 275:849–861.
61. Ohno Y, Yoshikawa T, Kishida Y, et al. Diagnostic performance of different imaging modalities in the assessment of distant metastasis and local recurrence of tumor in patients with non-small cell lung cancer. J Magn Reson Imaging 2017; 46:1707–1717.
62. Ohno Y, Kishida Y, Seki S, et al. Comparison of interobserver agreement and diagnostic accuracy for IASLC/ITMIG thymic epithelial tumor staging among co-registered FDG-PET/MRI, whole-body MRI, integrated FDG-PET/CT, and conventional imaging examination with and without contrast media administrations. Acad Radiol 2018 Feb 1. doi: 10.1016/j.acra.2017.12.016. [Epub ahead of print]
63. Ohno Y, Yui M, Aoyagi K, et al. Whole-Body MRI: comparison of its capability for TNM staging of malignant pleural mesothelioma with that of coregistered PET/MRI, integrated FDG PET/CT, and conventional imaging. AJR Am J Roentgenol 2019; 212:311–319.
64. Ohno Y, Takeshi Y, Takenaka D, et al. Comparison of diagnostic accuracy for TNM stage among whole-body MRI and coregistered PET/MRI Using 1.5-T and 3-T MRI systems and integrated PET/CT for non-small cell lung cancer. AJR Am J Roentgenol 2020; 215:1191–1198.
65. Vogt FM, Herborn CU, Hunold P, et al. HASTE MRI versus chest radiography in the detection of pulmonary nodules: comparison with MDCT. AJR Am J Roentgenol 2004; 183:71–78.
66. Bruegel M, Gaa J, Woertler K, et al. MRI of the lung: value of different turbo spin-echo, single-shot turbo spin-echo, and 3D gradient-echo pulse sequences for the detection of pulmonary metastases. J Magn Reson Imaging 2007; 25:73–81.
67. Yi CA, Jeon TY, Lee KS, et al. 3-T MRI: usefulness for evaluating primary lung cancer and small nodules in lobes not containing primary tumors. AJR Am J Roentgenol 2007; 189:386–392.
68. Koyama H, Ohno Y, Kono A, et al. Quantitative and qualitative assessment of non-contrast-enhanced pulmonary MR imaging for management of pulmonary nodules in 161 subjects. Eur Radiol 2008; 18:2120–2131.
69. Frericks BB, Meyer BC, Martus P, et al. MRI of the thorax during whole-body MRI: evaluation of different MR sequences and comparison to thoracic multidetector computed tomography (MDCT). J Magn Reson Imaging 2008; 27:538–545.
70. Cieszanowski A, Lisowska A, Dabrowska M, et al. MR imaging of pulmonary nodules: detection rate and accuracy of size estimation in comparison to computed tomography. PLoS One 2016; 11:e0156272.
71. Burris NS, Johnson KM, Larson PE, et al. Detection of small pulmonary nodules with ultrashort echo time sequences in oncology patients by using a PET/MR system. Radiology 2016; 278:239–246.
72. Li B, Li Q, Chen C, et al. A systematic review and meta-analysis of the accuracy of diffusion-weighted MRI in the detection of malignant pulmonary nodules and masses. Acad Radiol 2014; 21:21–29.
73. Basso Dias A, Zanon M, Altmayer S, et al. Fluorine 18-FDG PET/CT and diffusion-weighted MRI for malignant versus benign pulmonary lesions: a meta-analysis. Radiology 2019; 290:525–534.
74. Usuda K, Sagawa M, Motono N, et al. Diagnostic performance of diffusion weighted imaging of malignant and benign pulmonary nodules and masses: comparison with positron emission tomography. Asian Pac J Cancer Prev 2014; 15:4629–4635.
75. Koyama H, Ohno Y, Seki S, et al. Value of diffusion-weighted MR imaging using various parameters for assessment and characterization of solitary pulmonary nodules. Eur J Radiol 2015; 84:509–515.
76. Ohno Y, Kishida Y, Seki S, et al. Amide proton transfer-weighted imaging to differentiate malignant from benign pulmonary lesions: comparison with diffusion-weighted imaging and FDG-PET/CT. J Magn Reson Imaging 2018; 47:1013–1021.
77. Hittmair K, Eckersberger F, Klepetko W, et al. Evaluation of solitary pulmonary nodules with dynamic contrast-enhanced MR imaging—a promising technique. Magn Reson Imaging 1995; 13:923–933.

78. Gückel C, Schnabel K, Deimling M, et al. Solitary pulmonary nodules: MR evaluation of enhancement patterns with contrast-enhanced dynamic snapshot gradient-echo imaging. Radiology 1996; 200:681–686.
79. Ohno Y, Hatabu H, Takenaka D, et al. Solitary pulmonary nodules: potential role of dynamic MR imaging in management initial experience. Radiology 2002; 224:503–511.
80. Schaefer JF, Vollmar J, Schick F, et al. Solitary pulmonary nodules: dynamic contrast-enhanced MR imaging—perfusion differences in malignant and benign lesions. Radiology 2004; 232:544–553.
81. Kono R, Fujimoto K, Terasaki H, et al. Dynamic MRI of solitary pulmonary nodules: comparison of enhancement patterns of malignant and benign small peripheral lung lesions. AJR Am J Roentgenol 2007; 188:26–36.
82. Ohno Y, Koyama H, Takenaka D, et al. Dynamic MRI, dynamic multidetector-row computed tomography (MDCT), and coregistered 2-[fluorine-18]-fluoro-2-deoxy-D-glucose-positron emission tomography (FDG-PET)/CT: comparative study of capability for management of pulmonary nodules. J Magn Reson Imaging 2008; 27:1284–1295.
83. Zou Y, Zhang M, Wang Q, et al. Quantitative investigation of solitary pulmonary nodules: dynamic contrast-enhanced MRI and histopathologic analysis. AJR Am J Roentgenol 2008; 191:252–259.
84. Coolen J, Vansteenkiste J, De Keyzer F, et al. Characterisation of solitary pulmonary lesions combining visual perfusion and quantitative diffusion MR imaging. Eur Radiol 2014; 24:531–541.
85. Ohno Y, Nishio M, Koyama H, et al. Solitary pulmonary nodules: comparison of dynamic first-pass contrast-enhanced perfusion area-detector CT, dynamic first-pass contrast-enhanced MR imaging, and FDG PET/CT. Radiology 2015; 274:563–575.
86. Ohno Y, Fujisawa Y, Yui M, et al. Solitary pulmonary nodule: comparison of quantitative capability for differentiation and management among dynamic CE-perfusion MRI at 3 T system, dynamic CE-perfusion ADCT and FDG-PET/CT. Eur J Radiol 2019; 115:22–30.
87. Cronin P, Dwamena BA, Kelly AM, et al. Solitary pulmonary nodules: meta-analytic comparison of cross-sectional imaging modalities for diagnosis of malignancy. Radiology 2008; 246:772–782.
88. Sakai S, Murayama S, Murakami J, et al. Bronchogenic carcinoma invasion of the chest wall: evaluation with dynamic cine MRI during breathing. J Comput Assist Tomogr 1997; 21:595–600.
89. Ohno Y, Adachi S, Motoyama A, et al. Multiphase ECG-triggered 3D contrast-enhanced MR angiography: utility for evaluation of hilar and mediastinal invasion of bronchogenic carcinoma. J Magn Reson Imaging 2001; 13:215–224.
90. Tang W, Wu N, OuYang H, et al. The presurgical T staging of non-small cell lung cancer: efficacy comparison of 64-MDCT and 3.0 T MRI. Cancer Imaging 2015; 15:14.
91. Takenaka D, Ohno Y, Hatabu H, et al. Differentiation of metastatic versus non-metastatic mediastinal lymph nodes in patients with non-small cell lung cancer using respiratory-triggered short inversion time inversion recovery (STIR) turbo spin-echo MR imaging. Eur J Radiol 2002; 44:216–224.
92. Ohno Y, Hatabu H, Takenaka D, et al. Metastases in mediastinal and hilar lymph nodes in patients with non-small cell lung cancer: quantitative and qualitative assessment with STIR turbo spin-echo MR imaging. Radiology 2004; 231:872–879.
93. Ohno Y, Koyama H, Nogami M, et al. STIR turbo SE MR imaging vs. coregistered FDG-PET/CT: quantitative and qualitative assessment of N-stage in non-small-cell lung cancer patients. J Magn Reson Imaging 2007; 26:1071–1080.
94. Hasegawa I, Boiselle PM, Kuwabara K, et al. Mediastinal lymph nodes in patients with non-small cell lung cancer: preliminary experience with diffusion-weighted MR imaging. J Thorac Imaging 2008; 23:157–161.
95. Nomori H, Mori T, Ikeda K, et al. Diffusion-weighted magnetic resonance imaging can be used in place of positron emission tomography for N staging of non-small cell lung cancer with fewer false-positive results. J Thorac Cardiovasc Surg 2008; 135:816–822.
96. Morikawa M, Demura Y, Ishizaki T, et al. The effectiveness of ^{18}F-FDG PET/CT combined with STIR MRI for diagnosing nodal involvement in the thorax. J Nucl Med 2009; 50:81–87.
97. Nakayama J, Miyasaka K, Omatsu T, et al. Metastases in mediastinal and hilar lymph nodes in patients with non-small cell lung cancer: quantitative assessment with diffusion-weighted magnetic resonance imaging and apparent diffusion coefficient. J Comput Assist Tomogr 2010; 34:1–8.
98. Usuda K, Zhao XT, Sagawa M, et al. Diffusion-weighted imaging is superior to positron emission tomography in the detection and nodal assessment of lung cancers. Ann Thorac Surg 2011; 91:1689–1695.
99. Ohno Y, Koyama H, Yoshikawa T, et al. N stage disease in patients with non-small cell lung cancer: efficacy of quantitative and qualitative assessment with STIR turbo spin-echo imaging, diffusion-weighted MR imaging, and fluorodeoxyglucose PET/CT. Radiology 2011; 261:605–615.
100. Ohno Y, Koyama H, Yoshikawa T, et al. Diffusion-weighted MR imaging using FASE sequence for 3T MR system: Preliminary comparison of capability for N-stage assessment by means of diffusion-weighted MR imaging using EPI sequence, STIR FASE imaging and FDG PET/CT for non-small cell lung cancer patients. Eur J Radiol 2015; 84:2321–2331.
101. Usuda K, Maeda S, Motono N, et al. Diagnostic performance of diffusion-weighted imaging for multiple hilar and mediastinal lymph nodes with FDG accumulation. Asian Pac J Cancer Prev 2015; 16:6401–6406.
102. Nomori H, Cong Y, Sugimura H, et al. Diffusion-weighted imaging can correctly identify false-positive lymph nodes on positron emission tomography in non-small cell lung cancer. Surg Today 2016; 46:1146–1151.
103. Peerlings J, Troost EG, Nelemans PJ, et al. The diagnostic value of MR imaging in determining the lymph node status of patients with non-small cell lung cancer: a meta-analysis. Radiology 2016; 281:86–98.
104. Sommer G, Wiese M, Winter L, et al. Preoperative staging of non-small-cell lung cancer: comparison of whole-body

diffusion-weighted magnetic resonance imaging and 18F-fluorodeoxyglucose-positron emission tomography/computed tomography. Eur Radiol 2012; 22:2859–2867.
105. Schaarschmidt BM, Grueneisen J, Metzenmacher M, et al. Thoracic staging with ^{18}F-FDG PET/MR in non-small cell lung cancer – does it change therapeutic decisions in comparison to ^{18}F-FDG PET/CT? Eur Radiol 2017; 27:681–688.
106. Lee SM, Goo JM, Park CM, et al. Preoperative staging of non-small cell lung cancer: prospective comparison of PET/MR and PET/CT. Eur Radiol 2016; 26:3850–3857.
107. Takahashi K, Al-Janabi NJ. Computed tomography and magnetic resonance imaging of mediastinal tumors. J Magn Reson Imaging 2010; 32:1325–1339.
108. Inaoka T, Takahashi K, Iwata K, Nagasawa K, Shuke N, Aburano T., et al. Evaluation of normal fatty replacement of the thymus with chemical-shift MR imaging for identification of the normal thymus. J Magn Reson Imaging 2005; 22:341–346.
109. Linegar AG, Odell JA, Fennell WM, et al. Massive thymic hyperplasia. Ann Thorac Surg 1993; 55:1197–1201.
110. Takahashi K, Inaoka T, Murakami N, et al. Characterization of the normal and hyperplastic thymus on chemical-shift MR imaging. AJR Am J Roentgenol 2003; 180:1265–1269.
111. Inaoka T, Takahashi K, Mineta M, et al. Thymic hyperplasia and thymus gland tumors: differentiation with chemical shift MR imaging. Radiology 2007; 243:869–876.
112. Seki S, Koyama H, Ohno Y, et al. Diffusion-weighted MR imaging vs. multi-detector row CT: direct comparison of capability for assessment of management needs for anterior mediastinal solitary tumors. Eur J Radiol 2014; 83:835–842.
113. Yabuuchi H, Matsuo Y, Abe K, et al. Anterior mediastinal solid tumours in adults: characterisation using dynamic contrast-enhanced MRI, diffusion-weighted MRI, and FDG-PET/CT. Clin Radiol 2015; 70:1289–1298.
114. Falaschi F, Battolla L, Mascalchi M, et al. Usefulness of MR signal intensity in distinguishing benign from malignant pleural disease. AJR Am J Roentgenol 1996; 166:963–968.
115. Robinson BW, Lake RA. Advances in malignant mesothelioma. N Engl J Med 2005; 353:1591–1603.
116. Curran D, Sahmoud T, Therasse P, et al. Prognostic factors in patients with pleural mesothelioma: the European Organization for Research and Treatment of Cancer experience. J Clin Oncol 1998; 16:145–152.
117. Helm EJ, Matin TN, Gleeson FV. Imaging of the pleura. J Magn Reson Imaging 2010; 32:1275–1286.
118. Hierholzer J, Luo L, Bittner RC, et al. MRI and CT in the differential diagnosis of pleural disease. Chest 2000; 118:604–609.
119. Heelan RT, Rusch VW, Begg CB, et al. Staging of malignant pleural mesothelioma: comparison of CT and MR imaging. AJR Am J Roentgenol 1999; 172:1039–1047.
120. Patz EF, Shaffer K, Piwnica-Worms DR, et al. Malignant pleural mesothelioma: value of CT and MR imaging in predicting resectability. AJR Am J Roentgenol 1992; 159:961–966.
121. Sugarbaker DJ, Flores RM, Jaklitsch MT, et al. Resection margins, extrapleural nodal status, and cell type determine postoperative long-term survival in trimodality therapy of malignant pleural mesothelioma: results in 183 patients. J Thorac Cardiovasc Surg 1999; 117:54–63; discussion 63-65.
122. Gill RR, Umeoka S, Mamata H, et al. Diffusion-weighted MRI of malignant pleural mesothelioma: preliminary assessment of apparent diffusion coefficient in histologic subtypes. AJR Am J Roentgenol 2010; 195:W125–130.
123. Murphy DJ, Mak SM, Mallia A, et al. Loco-regional staging of malignant pleural mesothelioma by integrated ^{18}F-FDG PET/MRI. Eur J Radiol 2019; 115:46–52.
124. Hoeper MM, Bogaard HJ, Condliffe R, Frantz R, Khanna D, Kurzyna M, Langleben D, Manes A, Satoh T, Torres F, Wilkins MR, Badesch DB. Definitions and diagnosis of pulmonary hypertension. J Am Coll Cardiol 2013; 62(25 Suppl):D42–50.
125. Simonneau G, Montani D, Celermajer DS, et al. Haemodynamic definitions and updated clinical classification of pulmonary hypertension. Eur Respir J 2019; 53:1801913.
126. Galiè N, Humbert M, Vachiery JL, et al. ESC Scientific Document Group. 2015 ESC/ERS Guidelines for the diagnosis and treatment of pulmonary hypertension: The Joint Task Force for the Diagnosis and Treatment of Pulmonary Hypertension of the European Society of Cardiology (ESC) and the European Respiratory Society (ERS): Endorsed by: Association for European Paediatric and Congenital Cardiology (AEPC), International Society for Heart and Lung Transplantation (ISHLT). Eur Heart J 2016; 37: 67–119.
127. Kiely DG, Levin D, Hassoun P, et al. EXPRESS: Statement on imaging and pulmonary hypertension from the Pulmonary Vascular Research Institute (PVRI). Pulm Circ 2019; 9:2045894019841990.
128. Rajaram S, Swift AJ, Telfer A, et al. 3D contrast-enhanced lung perfusion MRI is an effective screening tool for chronic thromboembolic pulmonary hypertension: results from the ASPIRE Registry. Thorax 2013; 68:677–678.
129. Johns CS, Swift AJ, Rajaram S, et al. Lung perfusion: MRI vs. SPECT for screening in suspected chronic thromboembolic pulmonary hypertension. J Magn Reson Imaging 2017; 46:1693–1697.
130. Humbert M, Lau EM, Montani D, et al. Advances in therapeutic interventions for patients with pulmonary arterial hypertension. Circulation 2014; 130:2189–2208.
131. Swift AJ, Telfer A, Rajaram S, et al. Dynamic contrast-enhanced magnetic resonance imaging in patients with pulmonary arterial hypertension. Pulm Circ 2014; 4:61–70.
132. van Wolferen SA, Marcus JT, Boonstra A, et al. Prognostic value of right ventricular mass, volume, and function in idiopathic pulmonary arterial hypertension. Eur Heart J 2007; 28:1250–1257.
133. van Wolferen SA, van de Veerdonk MC, Mauritz GJ, et al. Clinically significant change in stroke volume in pulmonary hypertension. Chest 2011; 139:1003–1009.
134. van de Veerdonk MC, Kind T, Marcus JT, et al. Progressive right ventricular dysfunction in patients with pulmonary arterial hypertension responding to therapy. J Am Coll Cardiol 2011; 58:2511–2519.
135. Peacock AJ, Crawley S, McLure L, et al. Changes in right ventricular function measured by cardiac magnetic

resonance imaging in patients receiving pulmonary arterial hypertension-targeted therapy: the EURO-MR study. Circ Cardiovasc Imaging 2014; 7:107–114.
136. Ohno Y, Hatabu H, Murase K, et al. Quantitative assessment of regional pulmonary perfusion in the entire lung using three-dimensional ultrafast dynamic contrast-enhanced magnetic resonance imaging: preliminary experience in 40 subjects. J Magn Reson Imaging 2004; 20:353–365.
137. Ohno Y, Hatabu H, Murase K, et al. Primary pulmonary hypertension: 3D dynamic perfusion MRI for quantitative analysis of regional pulmonary perfusion. AJR Am J Roentgenol 2007; 188:48–56.
138. Ohno Y, Koyama H, Nogami M, et al. Dynamic perfusion MRI: capability for evaluation of disease severity and progression of pulmonary arterial hypertension in patients with connective tissue disease. J Magn Reson Imaging 2008; 28:887–899.
139. Ohno Y, Koyama H, Yoshikawa T, et al. Contrast-enhanced multidetector-row computed tomography vs. Time-resolved magnetic resonance angiography vs. contrast-enhanced perfusion MRI: assessment of treatment response by patients with inoperable chronic thromboembolic pulmonary hypertension. J Magn Reson Imaging 2012; 36:612–623.
140. Rajaram S, Swift AJ, Capener D, et al. Diagnostic accuracy of contrast-enhanced MR angiography and unenhanced proton MR imaging compared with CT pulmonary angiography in chronic thromboembolic pulmonary hypertension. Eur Radiol 2012; 22:310–317.
141. Swift AJ, Rajaram S, Condliffe R, et al. Pulmonary artery relative area change detects mild elevations in pulmonary vascular resistance and predicts adverse outcome in pulmonary hypertension. Invest Radiol 2012; 47:571–577.
142. Gan CT, Lankhaar JW, Westerhof N, et al. Noninvasively assessed pulmonary artery stiffness predicts mortality in pulmonary arterial hypertension. Chest 2007; 132:1906–1912.
143. Swift AJ, Capener D, Johns C, et al. Magnetic resonance imaging in the prognostic evaluation of patients with pulmonary arterial hypertension. Am J Respir Crit Care Med 2017; 196:228–239.
144. Baggen VJ, Leiner T, Post MC, et al. Cardiac magnetic resonance findings predicting mortality in patients with pulmonary arterial hypertension: a systematic review and meta-analysis. Eur Radiol 2016; 26:3771–3780.
145. de Siqueira ME, Pozo E, Fernandes VR, et al. Characterization and clinical significance of right ventricular mechanics in pulmonary hypertension evaluated with cardiovascular magnetic resonance feature tracking. J Cardiovasc Magn Reson 2016; 18:39.
146. Ray JC, Burger C, Mergo P, et al. Pulmonary arterial stiffness assessed by cardiovascular magnetic resonance imaging is a predictor of mild pulmonary arterial hypertension. Int J Cardiovasc Imaging 2019; 35:1881–1892.
147. Tello K, Dalmer A, Vanderpool R, et al. Right ventricular function correlates of right atrial strain in pulmonary hypertension: a combined cardiac magnetic resonance and conductance catheter study. Am J Physiol Heart Circ Physiol 2020; 318:H156–H164.
148. Sheh SH, Bellin E, Freeman KD, et al. Pulmonary embolism diagnosis and mortality with pulmonary CT angiography versus ventilation-perfusion scintigraphy: evidence of overdiagnosis with CT? AJR Am J Roentgenol 2012; 198:1340–1345.
149. Sikkens JJ, Beekman DG, Thijs A, et al. How much overtesting is needed to safely exclude a diagnosis? a different perspective on triage testing using Bayes' theorem. PLoS One 2016; 11:e0150891.
150. Ohno Y, Kawamitsu H, Higashino T, et al. Time-resolved contrast-enhanced pulmonary MR angiography using sensitivity encoding (SENSE). J Magn Reson Imaging 2003; 17:330–336.
151. Ohno Y, Higashino T, Takenaka D, et al. MR angiography with sensitivity encoding (SENSE) for suspected pulmonary embolism: comparison with MDCT and ventilation-perfusion scintigraphy. AJR Am J Roentgenol 2004; 183:91–98.
152. Kluge A, Luboldt W, Bachmann G. Acute pulmonary embolism to the subsegmental level: diagnostic accuracy of three MRI techniques compared with 16-MDCT. AJR Am J Roentgenol 2006; 187:W7–14.
153. Meaney JF, Weg JG, Chenevert TL, et al. Diagnosis of pulmonary embolism with magnetic resonance angiography. N Engl J Med 1997; 336:1422–1427.
154. Gupta A, Frazer CK, Ferguson JM, et al. Acute pulmonary embolism: diagnosis with MR angiography. Radiology 1999; 210:353–359.
155. Oudkerk M, van Beek EJ, Wielopolski P, et al. Comparison of contrast-enhanced magnetic resonance angiography and conventional pulmonary angiography for the diagnosis of pulmonary embolism: a prospective study. Lancet 2002; 359:1643–1647.
156. Stein PD, Chenevert TL, Fowler SE, et al. PIOPED III (Prospective Investigation of Pulmonary Embolism Diagnosis III) Investigators. Gadolinium-enhanced magnetic resonance angiography for pulmonary embolism: a multicenter prospective study (PIOPED III). Ann Intern Med 2010; 152:434-443, W142–143.
157. Rajaram S, Swift AJ, Capener D, et al. Lung morphology assessment with balanced steady-state free precession MR imaging compared with CT. Radiology 2012; 263:569–577.
158. Johnson KM, Fain SB, Schiebler ML, et al. Optimized 3D ultrashort echo time pulmonary MRI. Magn Reson Med 2013; 70:1241–1250.
159. Dournes G, Grodzki D, Macey J, et al. Quiet submillimeter MR imaging of the lung is feasible with a PETRA sequence at 1.5 T. Radiology 2015; 276:258–265.
160. Galbán CJ, Han MK, Boes JL, et al. Computed tomography-based biomarker provides unique signature for diagnosis of COPD phenotypes and disease progression. Nat Med 2012; 18:1711–1715.
161. Smith BM, Hoffman EA, Rabinowitz D, et al. Comparison of spatially matched airways reveals thinner airway walls in COPD. The Multi-Ethnic Study of Atherosclerosis (MESA) COPD Study and the Subpopulations and Intermediate Outcomes in COPD Study (SPIROMICS). Thorax 2014; 69:987–996.
162. Regan EA, Lynch DA, Curran-Everett D, et al. Genetic Epidemiology of COPD (COPDGene) Investigators. Clinical

and Radiologic Disease in Smokers With Normal Spirometry. JAMA Intern Med 2015; 175:1539–1549.
163. Putman RK, Hatabu H, Araki T, et al. Evaluation of COPD Longitudinally to Identify Predictive Surrogate Endpoints (ECLIPSE) Investigators; COPDGene Investigators. Association Between Interstitial Lung Abnormalities and All-Cause Mortality. JAMA 2016; 315:672–681.
164. Sack CS, Doney BC, Podolanczuk AJ, et al. Occupational Exposures and Subclinical Interstitial Lung Disease. The MESA (Multi-Ethnic Study of Atherosclerosis) Air and Lung Studies. Am J Respir Crit Care Med 2017; 196:1031–1039.
165. de Lange EE, Mugler JP, Brookeman JR, et al. Lung air spaces: MR imaging evaluation with hyperpolarized ^{3}He gas. Radiology 1999; 210:851–857.
166. Salerno M, de Lange EE, Altes TA, et al. Emphysema: hyperpolarized helium 3 diffusion MR imaging of the lungs compared with spirometric indexes–initial experience. Radiology 2002; 222:252–260.
167. Fain SB, Panth SR, Evans MD, et al. Early emphysematous changes in asymptomatic smokers: detection with 3He MR imaging. Radiology 2006; 239:875–883.
168. Quirk JD, Lutey BA, Gierada DS, et al. In vivo detection of acinar microstructural changes in early emphysema with ^{3}He lung morphometry. Radiology 2011; 260:866–874.
169. Kirby M, Mathew L, Heydarian M, et al. Chronic obstructive pulmonary disease: quantification of bronchodilator effects by using hyperpolarized ^{3}He MR imaging. Radiology 2011; 261:283–292.
170. Kirby M, Svenningsen S, Owrangi A, et al. Hyperpolarized 3He and 129Xe MR imaging in healthy volunteers and patients with chronic obstructive pulmonary disease. Radiology 2012; 265:600–610.
171. Kirby M, Pike D, Coxson HO, et al. Hyperpolarized (3)He ventilation defects used to predict pulmonary exacerbations in mild to moderate chronic obstructive pulmonary disease. Radiology 2014; 273:887–896.
172. Kirby M, Pike D, Sin DD, et al. COPD: do imaging measurements of emphysema and airway disease explain symptoms and exercise capacity? Radiology 2015; 277:872–880.
173. Westcott A, Capaldi DPI, McCormack DG, et al. Chronic obstructive pulmonary disease: thoracic CT texture analysis and machine learning to predict pulmonary ventilation. Radiology 2019; 293:676–684.
174. MacNeil JL, Capaldi DPI, Westcott AR, et al. Pulmonary imaging phenotypes of chronic obstructive pulmonary disease using multiparametric response maps. Radiology 2020; 295:227–236.
175. Tafti S, Garrison WJ, Mugler JP, et al. Emphysema index based on hyperpolarized ^{3}He or ^{129}Xe diffusion MRI: performance and comparison with quantitative CT and pulmonary function tests. Radiology 2020; 297:201–210.
176. Ohno Y, Hatabu H, Takenaka D, et al. Dynamic oxygen-enhanced MRI reflects diffusing capacity of the lung. Magn Reson Med 2002; 47:1139–1144.
177. Ohno Y, Hatabu H, Higashino T, et al. Oxygen-enhanced MR imaging: correlation with postsurgical lung function in patients with lung cancer. Radiology 2005; 236:704–711.
178. Ohno Y, Koyama H, Nogami M, et al. Dynamic oxygen-enhanced MRI versus quantitative CT: pulmonary functional loss assessment and clinical stage classification of smoking-related COPD. AJR Am J Roentgenol 2008; 190: W93–99.
179. Ohno Y, Iwasawa T, Seo JB, et al. Oxygen-enhanced magnetic resonance imaging versus computed tomography: multicenter study for clinical stage classification of smoking-related chronic obstructive pulmonary disease. Am J Respir Crit Care Med 2008; 177:1095–1102.
180. Ohno Y, Nishio M, Koyama H, et al. Oxygen-enhanced MRI, thin-section MDCT, and perfusion SPECT/CT: comparison of clinical implications to patient care for lung volume reduction surgery. AJR Am J Roentgenol 2012; 199:794–802.
181. Ohno Y, Koyama H, Yoshikawa T, et al. Comparison of capability of dynamic O_2-enhanced MRI and quantitative thin-section MDCT to assess COPD in smokers. Eur J Radiol 2012; 81:1068–1075.
182. Morgan AR, Parker GJ, Roberts C, et al. Feasibility assessment of using oxygen-enhanced magnetic resonance imaging for evaluating the effect of pharmacological treatment in COPD. Eur J Radiol 2014; 83:2093–2101.
183. Fuseya Y, Muro S, Sato S, et al. Complementary regional heterogeneity information from COPD patients obtained using oxygen-enhanced MRI and chest CT. PLoS One 2018; 13:e0203273.
184. Ohno Y, Yui M, Yoshikawa T, et al. 3D oxygen-enhanced MRI at 3T MR system: comparison with thin-section CT of quantitative capability for pulmonary functional loss assessment and clinical stage classification of COPD in smokers. J Magn Reson Imaging 2021; 53:1042–1051.
185. Gutberlet M, Kaireit TF, Voskrebenzev A, et al. Free-breathing dynamic ^{19}F gas MR imaging for mapping of regional lung ventilation in patients with COPD. Radiology 2018; 286:1040–1051.
186. Gutberlet M, Kaireit TF, Voskrebenzev A, et al. Repeatability of regional lung ventilation quantification using fluorinated ^{19}F gas magnetic resonance imaging. Acad Radiol 2019; 26:395–403.
187. Amundsen T, Torheim G, Waage A, et al. Perfusion magnetic resonance imaging of the lung: characterization of pneumonia and chronic obstructive pulmonary disease. A feasibility study. J Magn Reson Imaging 2000; 12:224–231.
188. Ohno Y, Hatabu H, Higashino T, et al. Dynamic perfusion MRI versus perfusion scintigraphy: prediction of postoperative lung function in patients with lung cancer. AJR Am J Roentgenol 2004; 182:73–78.
189. Ohno Y, Koyama H, Nogami M, et al. Postoperative lung function in lung cancer patients: comparative analysis of predictive capability of MRI, CT, and SPECT. AJR Am J Roentgenol 2007; 189:400–408.
190. Ohno Y, Koyama H, Nogami M, et al. State-of-the-art radiological techniques improve the assessment of postoperative lung function in patients with non-small cell lung cancer. Eur J Radiol 2011; 77:97–104.
191. Fan L, Xia Y, Guan Y, et al. Capability of differentiating smokers with normal pulmonary function from COPD

patients: a comparison of CT pulmonary volume analysis and MR perfusion imaging. Eur Radiol 2013; 23:1234–1241.
192. Hueper K, Parikh MA, Prince MR, et al. Quantitative and semiquantitative measures of regional pulmonary microvascular perfusion by magnetic resonance imaging and their relationships to global lung perfusion and lung diffusing capacity: the multiethnic study of atherosclerosis chronic obstructive pulmonary disease study. Invest Radiol 2013; 48:223–230.
193. Hueper K, Vogel-Claussen J, Parikh MA, et al. Pulmonary microvascular blood flow in mild chronic obstructive pulmonary disease and emphysema. The MESA COPD Study. Am J Respir Crit Care Med 2015; 192:570–580.
194. Schoenfeld C, Cebotari S, Hinrichs J, et al. MR Imaging-derived Regional Pulmonary Parenchymal Perfusion and Cardiac Function for Monitoring Patients with Chronic Thromboembolic Pulmonary Hypertension before and after Pulmonary Endarterectomy. Radiology 2016; 279:925–934.
195. Qing K, Tustison NJ, Mugler JP, et al. Probing Changes in Lung Physiology in COPD Using CT, Perfusion MRI, and Hyperpolarized Xenon-129 MRI. Acad Radiol 2019; 26:326–334.
196. Vogel-Claussen J, Schönfeld CO, Kaireit TF, et al. Effect of Indacaterol/Glycopyrronium on Pulmonary Perfusion and Ventilation in Hyperinflated Patients with Chronic Obstructive Pulmonary Disease (CLAIM). A Double-Blind, Randomized, Crossover Trial. Am J Respir Crit Care Med 2019; 199:1086–1096.
197. Ogasawara N, Suga K, Zaki M, et al. Assessment of lung perfusion impairment in patients with pulmonary artery-occlusive and chronic obstructive pulmonary diseases with noncontrast electrocardiogram-gated fast-spin-echo perfusion MR imaging. J Magn Reson Imaging 2004; 20:601–611.
198. Ohno Y, Seki S, Koyama H, et al. 3D ECG- and respiratory-gated non-contrast-enhanced (CE) perfusion MRI for post-operative lung function prediction in non-small-cell lung cancer patients: a comparison with thin-section quantitative computed tomography, dynamic CE-perfusion MRI, and perfusion scan. J Magn Reson Imaging 2015; 42:340–353.
199. Voskrebenzev A, Gutberlet M, Kaireit TF, et al. Low-pass imaging of dynamic acquisitions (LIDA) with a group-oriented registration (GOREG) for proton MR imaging of lung ventilation. Magn Reson Med 2017; 78:1496–1505.
200. Voskrebenzev A, Gutberlet M, Klimeš F, et al. Feasibility of quantitative regional ventilation and perfusion mapping with phase-resolved functional lung (PREFUL) MRI in healthy volunteers and COPD, CTEPH, and CF patients. Magn Reson Med 2018; 79:2306–2314.
201. Kaireit TF, Voskrebenzev A, Gutberlet M, et al. Comparison of quantitative regional perfusion-weighted phase resolved functional lung (PREFUL) MRI with dynamic gadolinium-enhanced regional pulmonary perfusion MRI in COPD patients. J Magn Reson Imaging 2019; 49:1122–1132.
202. Behrendt L, Voskrebenzev A, Klimeš F, et al. Validation of automated perfusion-weighted phase-resolved functional lung (PREFUL)-MRI in patients with pulmonary diseases. J Magn Reson Imaging 2020; 52:103–114.
203. Woolcock AJ. Epidemiology of chronic airways disease. Chest 1989; 96(3 Suppl):302S–306S.
204. To T, Stanojevic S, Moores G, et al. Global asthma prevalence in adults: findings from the cross-sectional world health survey. BMC Public Health 2012; 12:204.
205. Altes TA, Powers PL, Knight-Scott J, et al. Hyperpolarized 3He MR lung ventilation imaging in asthmatics: preliminary findings. J Magn Reson Imaging 2001; 13:378–384.
206. Samee S, Altes T, Powers P, et al. Imaging the lungs in asthmatic patients by using hyperpolarized helium-3 magnetic resonance: assessment of response to methacholine and exercise challenge. J Allergy Clin Immunol 2003; 111:1205–1211.
207. Haczku A, Emami K, Fischer MC, et al. Hyperpolarized ^{3}He MRI in asthma measurements of regional ventilation following allergic sensitization and challenge in mice–preliminary results. Acad Radiol 2005; 12:1362–1370.
208. de Lange EE, Altes TA, Patrie JT, et al. Evaluation of asthma with hyperpolarized helium-3 MRI: correlation with clinical severity and spirometry. Chest 2006; 130:1055–1062.
209. de Lange EE, Altes TA, Patrie JT, et al. The variability of regional airflow obstruction within the lungs of patients with asthma: assessment with hyperpolarized helium-3 magnetic resonance imaging. J Allergy Clin Immunol 2007; 119:1072–1078.
210. Wang C, Altes TA, Mugler JP 3rd, et al. Assessment of the lung microstructure in patients with asthma using hyperpolarized 3He diffusion MRI at two time scales: comparison with healthy subjects and patients with COPD. J Magn Reson Imaging 2008; 28: 80–88.
211. de Lange EE, Altes TA, Patrie JT, et al. Changes in regional airflow obstruction over time in the lungs of patients with asthma: evaluation with 3He MR imaging. Radiology 2009; 250:567–575.
212. Svenningsen S, Kirby M, Starr D, et al. Hyperpolarized ^{3}He and ^{129}Xe MRI: differences in asthma before bronchodilation. J Magn Reson Imaging 2013; 38:1521–1530.
213. Johansson MW, Kruger SJ, Schiebler ML, et al. Markers of vascular perturbation correlate with airway structural change in asthma. Am J Respir Crit Care Med 2013; 188:167–178.
214. Ebner L, He M, Virgincar RS, et al. Hyperpolarized ^{129}Xenon Magnetic Resonance Imaging to Quantify Regional Ventilation Differences in Mild to Moderate Asthma: A Prospective Comparison Between Semiautomated Ventilation Defect Percentage Calculation and Pulmonary Function Tests. Invest Radiol 2017; 52:120–127.
215. Svenningsen S, Eddy RL, Lim HF, et al. Sputum Eosinophilia and Magnetic Resonance Imaging Ventilation Heterogeneity in Severe Asthma. Am J Respir Crit Care Med 2018; 197:876–884.
216. Eddy RL, Svenningsen S, Licskai C, et al. Hyperpolarized Helium 3 MRI in Mild-to-Moderate Asthma: Prediction of Postbronchodilator Reversibility. Radiology 2019; 293:212–220.
217. Ohno Y, Koyama H, Matsumoto K, et al. Oxygen-enhanced MRI vs. quantitatively assessed thin-section CT: pulmonary functional loss assessment and clinical stage classification of asthmatics. Eur J Radiol 2011; 77:85–91.
218. Ohno Y, Nishio M, Koyama H, et al. Asthma: comparison of dynamic oxygen-enhanced MR imaging and quantitative thin-section CT for evaluation of clinical treatment. Radiology 2014; 273:907–916.

219. Pinal-Fernandez I, Pineda-Sanchez V, Pallisa-Nuñez E, et al. Fast 1.5 T chest MRI for the assessment of interstitial lung disease extent secondary to systemic sclerosis. Clin Rheumatol 2016; 35:2339–2345.
220. Stadler A, Jakob PM, Griswold M, et al. T1 mapping of the entire lung parenchyma: Influence of respiratory phase and correlation to lung function test results in patients with diffuse lung disease. Magn Reson Med 2008; 59:96–101.
221. Buzan MT, Eichinger M, Kreuter M, et al. T2 mapping of CT remodelling patterns in interstitial lung disease. Eur Radiol 2015; 25:3167–3174.
222. Ohno Y, Nishio M, Koyama H, et al. Oxygen-enhanced MRI for patients with connective tissue diseases: comparison with thin-section CT of capability for pulmonary functional and disease severity assessment. Eur J Radiol 2014; 83:391-397.
223. Molinari F, Eichinger M, Risse F, Plathow C, Puderbach M, Ley S, Herth F, Bonomo L, Kauczor HU, Fink C. Navigator-triggered oxygen-enhanced MRI with simultaneous cardiac and respiratory synchronization for the assessment of interstitial lung disease. J Magn Reson Imaging 2007; 26:1523–1529.
224. Kaushik SS, Freeman MS, Yoon SW, et al. Measuring diffusion limitation with a perfusion-limited gas–hyperpolarized 129Xe gas-transfer spectroscopy in patients with idiopathic pulmonary fibrosis. J Appl Physiol (1985) 2014; 117:577–585.
225. Wang JM, Robertson SH, Wang Z, et al. Using hyperpolarized 129Xe MRI to quantify regional gas transfer in idiopathic pulmonary fibrosis. Thorax 2018; 73:21–28.
226. Weatherley ND, Stewart NJ, Chan HF, et al. Hyperpolarised xenon magnetic resonance spectroscopy for the longitudinal assessment of changes in gas diffusion in IPF. Thorax 2019; 74:500–502.
227. Chan HF, Collier GJ, Weatherley ND, et al. Comparison of *in vivo* lung morphometry models from 3D multiple b-value 3 He and 129 Xe diffusion-weighted MRI. Magn Reson Med 2019; 81:2959–2971.
228. Yi CA, Lee KS, Han J, et al. 3-T MRI for differentiating inflammation- and fibrosis-predominant lesions of usual and nonspecific interstitial pneumonia: comparison study with pathologic correlation. AJR Am J Roentgenol 2008; 190:878–885.